T-71-01356

NGR-36-003-064

DIVISION OF

FLUID, THERMAL AND AEROSPACE SCIENCES

SCHOOL OF ENGINEERING

CASE WESTERN RESERVE UNIVERSITY

UNIVERSITY CIRCLE • CLEVELAND, OHIO 44106

EXPERIMENTAL MEASUREMENTS OF GRID-INJECTION

TURBULENT FLOWS

Julian C. H. Liu, I. Greber, and H. K. Wiskind*

January 1971

*Deceased March 19, 1970

ABSTRACT

A combination of a grid and jet injection parallel to a main

flow was used to generate turbulence. Investigations were made of

the structure and characteristics of the resulting turbulent flow.

For all injection rates, the energy containing eddies of the

generated turbulence were found to have the same characteristic

length as the mesh size of the grid used. The turbulence Reynolds

number could be increased as much as fivefold by the use of injec-

tion. The inertial subrange with slope $-5/3$ on energy spectra

could be seen clearly at the highest injection rate.

An effort was made to make the mean velocity field as uniform

as possible as part of an attempt to make the turbulence field

homogeneous. Energy decay and spectra measurements were taken,

and the results were compared with the experimental results of

zero injection (standard grid turbulence) and with theories of

homogeneous turbulence.

Flows which were almost homogeneous were obtained at dis-

tances of 20 mesh lengths downstream of the grid. The results

of energy decay for zero injection showed excellent agreement

with the theories. When injection was used, the total turbulence

energy was increased, and the decay rate and microscales were

different from what would be expected from homogeneous turbulence
theories. The disagreement increases with increasing injection
rate.

ACKNOWLEDGMENTS

TABLE OF CONTENTS

LIST OF SYMBOLS

$A(r')$	element of area on sphere of radius r'.
AA', BB'	lateral traverse paths.
$\overline{a}$	over heat ratio.
D	diameter of hot wire.
$E(\vec{k})$	energy spectrum function in wave number space.
$E_1(f)$	one dimensional energy spectrum as function of frequency.
$F(r')$	two point velocity correlation function.
f	frequency.
IRP	injection rate percent.
$K(r')$	three point velocity correlation function.
k	wave number.
M	mesh length, spacing of grid rods.
n	exponent of decay law.
P_1, P_2	positions of longitudinal traverse paths.
P	pressure fluctuation.
Q_i	volume flowrate of injected air.
Q_t	total volume flow rate of main flow downstream of grid.
R	radius of downstream test section.
R_o	cold resistance of hot wire.
R_u	radius of upstream test section.
$R_{ij}(\vec{r}')$	velocity covariance tensor.
Re_{λ_g}	turbulence Reynolds number based on λ_g.
r	radial distance from axis of test section.

r'	separation distance of correlation function.
t	time.
t_σ	time of decay from virtual origin.
U	free stream velocity.
$\bar{U}$	mean velocity of flow downstream of grid.
u_i	velocity fluctuation.
$\sqrt{\overline{u_i^2}}$	root mean square of velocity fluctuation.
x	longitudinal distance coordinate.
x_o	position of virtual origin.
ρ	density of air.
λ	microscale.
ν	kinematic viscosity.

CHAPTER I

INTRODUCTION

The usual manner of generating turbulence for laboratory studies is through the use of a grid. Under the usual restrictions of size and laboratory conditions, the turbulence Reynolds number for grid generated turbulence is restricted to rather low values. In order to obtain higher turbulence Reynolds numbers, a different mechanism has been used recently. An array of jets is introduced in the downstream direction, and a turbulent flow is produced through interaction of the jets with the entrained flow from upstream of the grid. Turbulence energy levels higher than those of the standard grid turbulence with the same mesh Reynolds number can be obtained at sufficiently high jet velocities.

Grid turbulence has been studied very thoroughly, and the results for homogeneous and isotropic turbulence have been shown to agree with existing theories quite well. However not much is known about the jet injection turbulence. Interesting aspects of this experiment are the characteristics of the turbulence generated by the combined grid and air injection mechanism. Comparisons were also made between the experimental results and homogeneous turbulence theories. A similar experiment was made by Tennisseu (Ref. 1), who used the method of generating turbulence only by jet injection without grid.

The present experiment is an extension of the experiments done by Conger (Ref. 2) and by Luxenberg (Ref. 3). Conger has measured

concentration fluctuation, and Luxenberg, using Conger's injection device, has measured energy decay and spectrum. However, with the grid set up by Conger, the turbulence field obtained was not homogeneous and the velocity profiles were not uniform. Roughly approximate homogeneity was obtained only after 50 mesh lengths downstream of the grid. Both experiments were carried out in the region from 50 to 86 (end of the test section) mesh lengths. In the present experiment, more uniform velocity profiles were obtained, and reasonably homogeneous mean-velocity fields were obtained as close as 20 mesh lengths. The maximum injection rate was also increased in comparison with the values obtained by Luxenberg. Therefore in the present experiment, the turbulence was studied in a wider range of conditions. A brief investigation of the jet mixing process and uniformity of the velocity field was made. Energy decay and spectra were also measured for several different injection rates. The results and conclusions are presented in the two concluding sections.

CHAPTER II

EXPERIMENTAL EQUIPMENT

Most of the experimental equipment was adapted from the equipment used by Conger and by Luxenberg. The main difference in equipment used for this present experiment and the previous experiments are the test section and grid-injection system. Detailed descriptions are written in the following sections.

2-(1) Wind Tunnel and Test Section

A schematic of the wind tunnel, grid and test section is shown in Figure 1. Two test sections were placed on both upstream and downstream sides of the grid. Both sections are made of Plexiglass tubing. The upstream section is 5 inches long, 5-7/16 inches inside diameter; the downstream section is 4-1/3 feet long, 5-3/16 inches inside diameter, and the upstream end is slightly tapered, 1/4 inch in diameter in 5 inches length.

The wind tunnel body upstream of the test section is the same as that used by Conger and Luxenberg and consists of three units; a Hartzell axial vane blower, a smoothing section and a contraction section. The test sections are connected to the wind tunnel body at the exit of the contraction section.

The wind tunnel motor speed is controlled by a Westinghouse silicon rectifier which provides continuous control of the speed between 7 f.p.s. to 110 f.p.s. For detailed description of the wind tunnel configuration and the rectifier circuitry, see Ref. 3.

2-(2) Grid Injection System

The grid is made of two sets of round tubes perpendicular to
each other such that the resulting mesh is square. Small holes were
drilled in the tubes with the openings facing downstream. When air
is injected into the tubes, an array of jets is formed downstream
of the grid as air exits through the small orifices.

The tubes are 5/8 inches apart from center to center and the
outside diameter of the tubes is 5/32 inches yielding a mesh to
diameter ratio of 4. A top and cross sectional view of the grid is
shown in Figure 2.

The grid used by both Conger and Luxenberg was intended to
give a uniform velocity profile, which is necessary for creating
homogeneous turbulence, at downstream positions of 50 to 86 (end
of the test section) mesh lengths from the grid, but the velocity
profile obtained was not uniform and consequently the flow field
is too far from homogeneous flow field (Ref. 3). Therefore, for
the present experiment, it was desired to incorporate the following
improvements: first, a more efficient means of air injection for
generation of homogeneity and second, extension of the region of
homogeneity to cover 20 to 86 mesh lengths downstream of the grid.

It was thought there might be several variables related to the
grid which might affect the velocity profile while air is injected,
namely, (1) the distribution of the orifices and the distribution
of the sizes which give different momentum distributions, (2) the
inside diameter of the tubes, which might give sufficient effect

on pressure distribution along the tubes thus giving different velocities of the jets along each tube, (3) the wall thickness of the tubes which gives the length of guidance of the jet directions at each orifice. However, it was found that the last two variables only give very small effects while the first one gives the dominant effect. This made the task simpler in that only the distribution of hole size had to be changed. A suitable distribution for the desired flow condition was found by trial and error as was done by Conger. It was a very time consuming process. And since the jet velocities are very sensitive to size and position of the small orifices, much care had to be taken when drilling those holes.

The final form of the distribution which was used is shown in Figure 3. The size of the orifices, except the ones nearest to the wall, are uniform with 0.020 inches diameter and located at the center on each side of the squares formed by the tubes. The remaining twenty holes are about 1/16 inch from the wall and with two different sizes of 0.0135 and 0.0160 inches, the smaller holes being the ones closer to the uniform holes. The reason for this distribution of holes and hole sizes is to try to create a uniform distribution of injected momentum through the jets into the free stream.

2-(3) Air Supply System

The source of the air injected through the grid is an Allis Chalmers compressor driven by a 100 hp motor and which can supply 402 cubic feet of air per minute. The compressed air flows into a large accumulator before being discharged for experimental use.

The pressure is automatically regulated so that it stays between 85 and 95 psi. When using the air for experiments, there is a variation in pressure over this range with a period of about 15 minutes.

However, this pressure variation has to be eliminated since we need the jet velocities to be constant. Therefore, the volume flow rate injected must be constant. The variation in pressure also yields error in the air flowmeter readings. To eliminate the pressure variation, a constant pressure regulator and three constant flow rate regulators were used. First, the large fluctuations in pressure could be eliminated by the pressure regulator, but small fluctuations still remained. Thus, at the second stage, additional constant flow rate regulators are used to keep the volume flow rate constant.

The principle of the constant flow rate regulator is to keep the pressure difference across a small orifice constant (here at 3 psi), thus causing the flow passing through the orifice to be constant. With these settings, the fluctuation of the flowrate was accurate within ± 1% of set flowrate. The three constant flowrate regulators are connected in parallel. A total capacity of nine cubic feet per minute was obtained.

The orifices in the constant flow rate system are made of adjustable control valves. By adjusting the valves, different injection rates could be obtained. The pressure in the injection system between the grid and the constant flowrate regulator varies

when varying the flowrate regulator control valves, and it was not possible to eliminate this variation. However, this variation in pressure does not affect the running of the experiment; it only affected the flowmeter readings which were corrected utilizing information supplied by the manufacturer.

2-(4)   Hot Wire Probe and Anemometer

The hot wire used is made from 90% platinum - 10% rhodium Wallaston wire with a diameter of 0.0001 inch. The etched length is about 0.045 inch. Thus the length to diameter ratio is about 450.

The anemometer is a constant current hot wire set, Model 50, manufactured by the Shapiro and Edward Co. For detailed description see Ref. 3.

2-(5)   Wave Analyzer

The energy spectra are measured by a General Radio Model 1900A wave analyzer. The accuracy in the selected frequency is $\pm$ 2 CPS below 2KC and $\pm$ 5 CPS up to 50 KC. Measurements can be made in three different bandwidths, 3, 10 and 50 CPS. The voltage accuracy up to 50 KC is $\pm$ 3% of the indicated value + 2% of the full scale value.

2-(6)   Other Equipment

(1) A Fisher and Porter flowmeter was used between the constant flowrate regulator and the grid. The accuracy of the meter is $\pm$ 2% of the full scale deflection. The maximum flowrate is 33 SCFM at 14.7 psi.

(2) A Meriam 34 FB2 micromanometer was used for measuring velocity and static pressure. The accuracy is + 0.001 inch of water.

(3) A 60 inch vertical water manometer was also used for measuring the jet velocities.

(4) The time constant of the hot wire was determined by observing, on an oscilloscope (Tectronic 502A), the compensated wave form of a square wave signal injected through the hot wire.

2-(7) Probe Positioning Device

The probe positioning device was also adopted from the previous experiment performed by Luxenberg (Ref. 3). The probe holder is capable of being moved along the test section and rotated about the axis of the test section. Both the hot wire probe and the pitot static tube could be fastened on this holder. However, due to the structure of the holder, they cannot be positioned on the center line of the test section. In order to meet as closely as possible the required conditions, the two probes were put 3/4 inches off the centerline and 1-1/2 inches apart.

CHAPTER III

PROCEDURE FOR THE EXPERIMENTAL MEASUREMENTS

All experimental runs were taken under the condition that the mean velocity 20 mesh lengths downstream of the grid and at point P_1 (see Figure 3) be 20 feet per second. Velocity profiles were then determined at a series of positions downstream from the grid. Turbulence intensity measurements were taken at points P_1 and P_2 (see Figure 3). As can be seen in Figure 3, P_2 is located at the center of one of the jets and P_1 is located at the center of one of the square mesh of the grid. The reason for having chosen these two points in this manner was to enable observation of any possible difference between the flow of the free stream through grid and flow directly downstream of the jets. Both points P_1 and P_2 which were used for intensity measurements also satisfied the criterion that the velocity gradients in an interval centered about these points in average along the whole length of the test section be small in comparison to the velocity gradients of the rest of the profile. This criterion is essential for the flatness of the velocity profiles which is an initial requirement in having homogeneity of the flow field.

3-(1) Setting Desired Condition

Measurements were taken at 6 different conditions: five with different injection rates and one without injection. As the injection rate increased, the wind tunnel fan speed had to be decreased to maintain the main stream velocity constant. The velocity was

kept constant of 20 f.p.s. at 20 mesh lengths downstream of the grid.
At the indicated injection rate of 7.85 cubic feet of air per minute,
the wind tunnel fan had to be stopped in order to maintain the main
stream velocity constant. At injection rates higher than this, the
situation arose that the fan should be running in reverse to main-
tain 20 f.p.s. downstream. However, the control system of the
tunnel did not permit reverse operation. Consequently, a second
method was utilized blocking the inlet area of the wind tunnel.

Before each experimental run, the motor of the wind tunnel
was kept running at least two hours so that the temperature of the
motor could reach equilibrium and the speed would remain constant.
Also the constant flowrate regulator requires some time to reach
equilibrium condition after each new setting. Therefore, at least
half of an hour was allowed between measurements after a new setting.

3-(2) Velocity Profile and Static Pressure Measurements

Velocity profiles were measured by small total head tubes
inserted through the wall of the test section. The hot wire probe
and pitot static tube were put inside the test section to keep the
static pressure the same as when taking hot wire measurements.
Still, it is impossible to keep the static pressure exactly con-
stant. When traversing with the hot wire probe, pressure will be
changed because of the varying probe interference. However, extreme
care was taken to try to keep the pressure as constant as possible.

The total head tubes were made of hypodermic needles with
0.025 inch diameters. The probe was moved laterally at a fixed
distance from the grid for each profile measurement.

Measurements were taken with spacing of 1/64 inch to 10/64 inch depending on how fast the velocity changed in the region being probed. Since the jet velocity was very high, the velocity would change from 150 f.p.s. to 5 f.p.s. within 5/64 inch at the distance 10 orifice diameter downstream of the grid. Thus the measurements were taken mostly with 1/64 inch spacing close to the grid. This is a very time consuming process. Often one traverse along the diameter would take 8 to 9 hours.

Mean static pressures used for calculating the velocities were taken by the pitot static tube set at the same distance from the grid. The pressure is assumed constant at any given cross section, except in the region closer than 10 orifice diameters from the grid. In this region close to the grid the pressure is one constant in the low pressure wake regions of the rods and another constant outside the wakes.

The velocity profiles were measured along two perpendicular traverse paths at distances of 10 and 20 times the diameter of the orifices, and at 2.15, 4.9, 10, 19.5, 31.1 and 86 (end of test section) mesh lengths. The traverse paths were put on the same planes AA' and BB' (shown in Figure 3) in order to detect the general change of the velocity profiles downstream along the test section. The traverse plane BB' is along a diameter and directly downstream of a grid tube, and the traverse plane AA' is displaced 5/16 inch from a plane formed by a diameter of the test section and is midway between two grid tubes. The above mentioned arrange-ment is for the purpose of observing any possible difference in

velocity profile at a cross section.

It was planned that such measurements be taken at all the eight positions in all conditions. But because the process was so time consuming, it was decided to take measurements only at two different injection rates of 3.5 and 7.85 cubic feet per second.

Static pressure distributions along the test section length were measured for each different injection rate by moving the pitot static tube longitudinally through the test section.

3-(3) <u>General Procedure for Hot Wire Measurements</u>

The hot wires were made by an etching process. Each hot wire

was inspected under a microscope after etching. For good performance,

the etched part must be straight and clean.

Each hot wire was calibrated before being used for taking

measurements. Calibration runs were taken in the upstream test

section where the turbulence of the stream is small. An over heat

ratio, defined as the ratio of the temperature increase of the hot

wire due to heating to the unheated wire temperature, was chosen

as 0.3   Since the calibration curve deviates slightly from a

straight line for higher velocities, a range of velocities between

10 and 50 f.p.s. was chosen for calibration purpose.

Because of the drifting phenomenon of the hot wire, calibration

has to be taken only after equilibrium at 0.3 overheat ratio

had been reached. Usually it takes 1 to 2 hours to reach

equilibrium.   Also half an hour between each new measurement at

the overheat ratio of 0.3 was permitted to eliminate any effect due

to small amount of drift.

The hot wire calibration equation is expressed by

$$\frac{i^2}{i_o^2} = \sqrt{\frac{U}{U_o}} + 1$$

deduced from King's Law (Ref. 4) for constant overheat ratio, i is

the current through the hot wire and U is the velocity of the flow

field. Measurements of U and i were made enabling the constants

i_o and U_o to be determined, for later use in turbulence intensity measurements:

The response of the hot wire to temperature changes depends on the time constant of the wire. The time constants for the hot wires used are between 200 microseconds and 500 microseconds. The corresponding maximum frequency responses are from only 350 to 800 cycles per second approximately. Therefore, compensation for the thermal inertial effect had to be used.

A specification of the increase of frequency by compensation is called "floor to ceiling ratio," defined as the ratio of the time constant of the hot wire, T_w, to the time constant of the anemometer circuit, T_c. The time constant of the circuit or hot wire is defined as $T_c = \frac{1}{2 \pi f}$ where f is the frequency of a sine wave signal injected through the circuit or hot wire such that the ratio of the input to output peak voltage is 0.707. The ratio of the anemometer used is 500. Thus, the compensated output signal could respond to the signal of temperature variation at the hot wire to 70.7 percent, up to between 1.75×10^5 and 4×10^5 cycles per second. However, due to the noise effect and the accuracy of the compensated signal, the range of frequency was limited to from 1 CPS to 5 KCPS. But the contribution to the turbulence energy is very small at very high frequency. Thus, this range is still sufficient for the study of the main characteristics of turbulence energy.

3-(4) Energy Decay Measurements

The velocity profile measurements indicated that between 15 and 20 mesh lengths downstream of the grid, the jets and free stream are

fully mixed. Beyond this length downstream of the grid, a homo-geneous condition may occur. Energy decay measurements were taken in an interval of 15 to 70 mesh lengths downstream of the grid.

In addition, the velocity profile measurements indicated that the best position for energy decay measurements was along longitud-inal lines displaced 3/4 inch from the centerline of the test section. The locations of the lines on a cross section of the test section are shown in Figure 3 as P_1 and P_2. Along these lines, the pitot static and hot wire probes were immersed in flows for which the condition of homogeneity was most nearly satisfied.

Between 15 and 35 mesh lengths downstream of the grid, measure-ments were taken every 2.5 mesh lengths. Downstream of 35 mesh lengths, measurements were taken every 5 mesh lengths.

Traverses were also taken along the two longitudinal paths parallel to the centerline of the test section and passing through the points P_1 and P_2. Both velocity and turbulence intensity were measured at the same points by rotating the probe to that point at each position.

The anemometer output readings were displayed on a mean square voltmeter. The meter was calibrated after each run by means of a square wave generator included as one part of the anemometer.

3-(5)   <u>Energy· Spectrum Measurements</u>

At 25 and 50 meshlengths downstream of the grid, energy spectra
measurements were taken at each injection rate so that changes in
spectra due to varying injection flow as well as changes in spectra
due to decay were observed.

The operation of the hot wire probe and anemometer for spectra
measurements was the same as for decay measurements except for the
addition of a wave analyzer. The signal from the output terminal
on the anemometer was fed to the analyzer and the readings were dis-
played on a RMS voltmeter on the wave analyzer.

The frequency dials of the analyzer were calibrated against
the frequency of the AC power supply and the voltmeter was calibrated
against an internal signal from the wave analyzer (Ref. 6).

For the purpose of neatness and convenience, the spacing in
frequency between test readings for each spectrum were chosen in
such a way that they would show about equal spacing on a logarithmic
scale. 20 voltage readings 10 seconds apart were taken for each
frequency chosen. An average of the 20 readings was utilized as
the true measured value.

20 CPS was chosen as the first point for each spectrum measure-
ment. For frequency below this value, the errors from the interval
circuits of the analyzer and vibration of the test facility
became large. The readings taken were terminated at 5000 CPS.
Again errors would be too large above this frequency due to the
noise pick-up. Measurements were all taken with a bandwidth of
3 cycles and the meter response slow.

CHAPTER IV

DISCUSSION OF ERRORS

Most of the velocities were measured with a micromanometer
which could be read to 0.0001 inches of water. The accuracy of reading is
within ± 0.0002 inches. Thus the maximum error is estimated as
being ± 2% of indicated value. The peak velocities of the jets at
a distance of 20 diameter of orifices downstream were measured by
a vertical manometer. The readings varied from 1.2 inches to 5
inches and the errors are estimated within 10% of the indicated
values. Static pressure measurements were also taken with the
micromanometer and with errors estimated to be ± 2% of indicated
value.

The readings of the mean square voltmeter on the hot wire
anemometer were taken by visual averaging. The meter was cali-
brated after each experimental run. During this calibration, errors
were involved from two sources. First, the reading of the mean
square voltmeter, which was estimated being within ± 0.5% of indi-
cated value. A second error was involved in the reading of the
meter which measured the voltage of the square wave signal used for
calibrating the M.S. meter. This second error was estimated being
within ± 1.0% of the RMS voltage of the square wave signal, which
corresponded to a ± 1.5% error shown on the mean square meter.
Thus a maximum error of ± 2% of indicated value on the mean square
meter existed for the calibration. A maximum estimated error due
to fluctuation of within ± 2% existed in reading of the mean square

meter during experimental measurements. Therefore, the total
maximum error of the root-mean-square value is within $\pm$ 2%.

The potentiometer and bridge were far more accurate than any
other segments of the hot wire circuitry. Therefore, any errors
introduced due to the use of these instruments was small compared
to those introduced in the reading and calibration of the mean
square output meter.

Close inspection of the hot wire calibration curve, Figure 4,
shows that the points actually form a slightly curved line rather
than a perfectly straight line. This results from the fact that
King's Law is not perfectly obeyed by the bridge output voltage.
By assuming a straight line, a slight error is introduced but it
is in no case greater than $\pm$ 2.5%.

The accuracy of the RMS voltmeter on the wave analyzer is
within $\pm$ 5% of full scale value. The readings were estimated
with errors within $\pm$ 2% of the indicated value.

Therefore an estimate of the total errors involved in energy
decay and energy spectra measurements is within $\pm$ 10% of the
true value.

CHAPTER V

DISCUSSION OF RESULTS

5-(1) Wind Tunnel and Grid Performance

The turbulence appearing in the downstream flow depends on

the volume flowrate of the air injected and the total volume flow-

rate downstream of the grid. An injection parameter is then

defined as

$$IRP = \frac{Q_i}{Q_t} \times 100\%$$

where Q_i is the volume flowrate of the injected air and Q_t is

the total volume flowrate of the main flow downstream of the grid.

Figure 5, a velocity profile taken upstream of the grid,

shows that the free stream velocity at the exit of the wind tunnel

is very uniform. This is a good foundation for generating homo-

geneous turbulent flows.

Figure 6 shows the velocity measurements with zero injection.

Wiggles are seen on the profile measured at 4.9 mesh lengths

downstream of the grid, but there is no wiggle appearing on the

profiles measured after 10 mesh lengths. This indicates that the

mixing process of the jets with the free stream is complete before

the position of 10 mesh lengths downstream of the grid.

The velocity profiles measured with injection are shown in

Figures 7, 8, 9, 10 and 11. For both injection rates IRP 1.88

and 4.99, mixing seems reasonably complete, as judged by uniformity

of the velocity, between 10 and 20 mesh lengths downstream of the
grid. The velocity distribution is not perfectly uniform, but
deviation from uniformity is within ± 5%.

Static pressure distributions along the test section length
were also measured along a line through the center of one mesh square
of the grid and parallel to the axis of the test section. Figure 12
shows that at zero injection rate the maximum pressure just upstream
of the grid is higher than the maximum pressure downstream of the
grid, whereas at sufficiently high injection rates the maximum
pressure upstream is lower than the maximum pressure downstream.
The figure also shows that downstream of the grid the pressure
decreases from its maximum value first at a relatively rapid rate
for a short distance, then at a slower almost constant rate for
most of the length of the test section, then again at a more
rapid rate near the end of the test section. It is seen that the
downstream static pressure distribution does not vary very much
with injection rate, except for a region near the grid.

The large pressure variations with injection rate in the
vicinity of the grid, both upstream and downstream, are the re-
sult of the detailed construction and operational features of the
tunnel. The decrease in maximum pressure upstream is due to
the fact that the speed of the wind tunnel fan had to be decreased
as the injection rate increased, in order to maintain the down-
stream speed constant at 20 feet per second (this was previously
mentioned in Section 3-1). The more rapid decrease of static

pressure in the downstream region close to the jet than farther downstream is apparently due to the slight taper of the test section in this region. Recall that the test section decreases its diameter from 5-7/16 inches to 5-3/16 inches in about 9 mesh lengths, which is also the region of rapid pressure decrease.

The arrows shown in all the velocity profile figures indicate the position of the pitot static and hot wire probes. The probes are seen to be immersed in sufficiently uniform velocity regions along the test section from 20 to 86 (end of test section) mesh lengths downstream of the grid for all different injection rates. Therefore, the region from 20 to 70 mesh lengths downstream of the grid was decided to be the region for turbulence measurements.

5-(2) Energy Decay

A general picture of the decay of the turbulence is shown in
Figure 13. This figure is constructed in the usual way by plotting
the inverse of the turbulence intensity $\frac{\overline{u^2}}{\overline{U^2}}$ versus the downstream
positions. To avoid confusion, only one set of data for each in-
jection rate is shown. The starting level of the curves is seen
to decrease with increasing injection rate. This means that the
starting energy level for each case is higher for higher injection
rates. The energy is also seen to gradually decrease toward the
right hand side along each curve. Utilizing Taylor's hypothesis,
this could be explained as the decay of turbulence energy with
time.

For zero injection rate case, the turbulence is generated
by the energy transfer between the grid and the free stream. As
the injection rate is increased, the turbulence generated due to
the jets also increases, and the jets gradually take over the role
of the main source of the turbulence. Turbulence energy is
generated as the jets spread and mix with the free stream. This
turbulence energy distributes into the main flow and consequently
increases the turbulence energy level in the main flow. The jets
formed by the injected air are generally turbulent. At the lowest
set injection rate, IRP 1.88, the Reynolds number of the jets at the
nozzle is about 1.4×10^4.

The curves in Figure 14, decay of turbulence energy with downstream

positions also show larger slopes for higher injections, which

means that the decay is faster for higher injections. It is import-

ant to find the decay rate with respect to time. With Taylor's

hypothesis, the decay rate can be determined graphically by con-

verting time to the distance downstream of the grid. The curves in

Figure 13 are evidently non-linear. Thus the same set of data was

first plotted with logarithmic scales (Figure 15), in anticipation

of finding the correct powers according to the general power decay

law (Appendix A).

Except for the zero injection case, Figure 15 shows that the

result for each other injection case does not follow a single

straight line. Each curve of injection data can be fitted approxi-

mately by two straight lines although the data actually forms

a curve with gradual change in slope. The downstream end sections

of the lines coincide closely with the results obtained by Luxen-

berg (Ref. 3). However, as a whole, the variation of the power

along each curve is considerably different from the results, in

the same range of positions, obtained by other persons. And since

the total process of decay lasts only less than 0.02 seconds, it

is not likely that two distinct decay rates exist. Therefore,

more basic considerations were utilized in treating the results.

A better way of plotting the result was found when trying

to verify basic decay laws. As mentioned in Appendix A, there are

two theories suggested by Lin and by Von Karman and Howarth.

Both theories are based on the assumption of self-preservation of

the energy spectrum during decay while the largest eddies almost

remain unchanged (Ref. 7). The results were therefore replotted

so that a proper comparison could be made with the above mentioned

theories.

With the assumption of full similarity of the energy spectrum

plus Loitsiansky's invariant, the decay law suggested by Von Karman

and Howarth is $\overline{u^2} = ct^{-n}$ where the time t is considered starting

from infinite turbulence energy, and from this point in time, the

energy decays according to the $-n$ power. This point is called the

virtual origin. Therefore, the decay curve should appear as a

straight line with slope $-n$ on a logarithmic scale if plotted from

the virtual origin.

The same set of data was then plotted again from the virtual

origin. The process was done by trial and error. Each curve was

plotted and tried with different starting positions. A final

form was chosen only for the one showing the best fit of the data

to a straight line. The final form for all the injection rates is

shown in Figure 16. The virtual origin and power was then deter-

mined by the starting position and the slope of each line.

The power n for different injection rates is shown in Table 1.

For zero injection rate cases, the power is 1.45 which agrees

closely with Kolmogaroff's $-10/7$ law. As the injection rate

increases, the power decreases to a minimum of 0.855 at an IRP

of 2.52 and then increases to a maximum of 3.37 at the highest in-

jection rate.

The value 3.37 is very much larger than the value of the decay

power for zero injection. It is also much larger than the results obtained both from the measurements of other workers in grid turbulence, and from theories of homogeneous turbulence. This seems to indicate that the turbulence generated by injection does not follow the homogeneous turbulence power decay law very well.

A second treatment was suggested by Lin with the assumption of only partial similarity, which is that the largest eddies play no role in the similarity of energy spectrum during decay and the similarity is determined only by a set of smaller eddies containing the bulk of the energy. According to his suggestion, the decay law is in the form $\overline{u^2} = a(t-t_o)^{-1} + b$. The constants

a, b and t_o were determined from the measured data. Figure 14 shows the same set of data but plotted with $\dfrac{\overline{u^2}}{\overline{U^2}}$ as the parameter for the convenience of the calculation. The solid lines are the calculated curves. The decay is shown in Figure 17 to have -1 power dependence when $\dfrac{\overline{u^2} - b}{\overline{U^2}}$ is plotted on the ordinate against $x/M - x_o/M$ on the abscissa. This seems to indicate that the decay follows Lin's decay law quite well.

However, it was found, in examining the microscale, that the result obtained from energy spectra measurement does not agree with the results deduced from Lin's decay law and from the general power decay law. Details are discussed in a later section.

The microscales λ_g and turbulence Reynolds numbers Re_{λ_g} obtained from both decay laws and from energy spectra are shown in Tables 1, 2 and 3. In general, both λ_g and Re_{λ_g} increase as the injection rate increases. The microscale increases during decay for each injection while the Reynolds number decreases. Details about the changing of microscales and turbulence Reynolds number will be discussed later together with the results from spectra measurements.

There is no evidence from the results to show that the decay agrees with Dryden's -1 power law (Appendix A). Actually, the -1 power is only a special case of both the general power law and Lin's decay law. But it was found from the present experiment that

the power n from the result obtained according to the general power

law does not equal 1 and b (from Lin's law) does not equal zero.

5-(3) Energy Spectrum

Figures 18, 19, 20 and 21 show the energy spectra measured at

25 and 50 mesh lengths downstream of the grid for each injection

rate. Figures 22 and 23 give a comparison for all of the different

injection rates at these two positions.

At high injection rates, a distinct portion of the curve is

seen to follow closely to the -5/3 power. According to Kolmogoroff's

theory, this portion of the curve is called the inertial subrange

of the universal equilibrium range. And this subrange is revealed

only when the Reynolds number is sufficiently large. It is seen

that the portion of the curve having this power decreases as injec-

tion decreases, and at the zero injection case there is no evidence

of any portion of the curve having a -5/3 power dependence. This

is interesting because it has been shown by Stewart and Townsend

that for an inertial subrange the mesh Reynolds number of grid

turbulence should be at least of the order of 10^6. The mesh Reynolds

number in this experiment is only about 6.5×10^3, but the subrange

is evident already.

However, it is important to recall that in the present experi-

ment, turbulence is not solely generated by the grid, so the mesh

Reynolds number is no longer proper for judgment of turbulence

generating device. But, after all, a big advantage of this kind of

grid injection device is the capability of increasing the turbulence

energy tremendously while the size of the device remains small and

the velocity of the flow remains reasonably low.

This -5/3 power was also observed by Luxenberg in his grid injection measurements (Ref. 3), but with less clarity than in this experiment. One reason may be that the highest injection rate he obtained was IRP = 4.15, while in the present experiment, a maximum injection rate IRP = 5.34 was obtained.

Close observation of Figure 22 and Figure 23 shows that for high injections, the curves tend to be higher in an interval near $k\lambda_g = 1.5 \times 10^{-1}$ and lower in an interval near $k\lambda_g = 1.$ However, these figures show only the normalized spectra, and we can only say that for higher injection rates, the energy for lower $k\lambda_g$ values is relatively higher than that for the no injection case. Since the region near $k\lambda_g = 1.5 \times 10^{-1}$ contains the highest energies, this could mean that the contribution to total energy is mostly from this region. Thus the eddies in this range could be considered as the energy containing eddies. Therefore, a more reasonable interpretation is that when air is injected into the main flow, turbulence energy is added into the stream and this turbulence is added predominantly to the eddies with size about $k\lambda_g = 1.5 \times 10^{-1}$.

It is expected that the characteristic length scale of the energy containing eddies should be about the size of the mesh of the grid or the spacing of the jets. In grid turbulent flow, the energy containing eddies starts in the wake behind the grid bars and they grow larger and larger downstream as the wake spreads. The growing stops when the eddies are about the same size as mesh and start interacting with similar eddies in the neighboring wakes.

For this reason, the size of the energy containing eddies generated by injection remains constant for varying injection rates. The mesh size of 0.625 inches corresponds to a wave number of 1.67 inch and therefore a $k\lambda_g$ value of about 0.165. The agreement with the corresponding value in Figures 22 and 23 is excellent.

One important purpose of the energy spectrum measurements is that they serve as a check on the validity of the decay laws followed by the turbulence generated by the grid and injection. Microscales and Reynolds numbers calculated directly from the spectrum data yield more direct information about the injection turbulent flow than microscales deduced from energy decay measurements.

For zero injection rate, the microscale values as calculated from the energy spectrum measurements and as calculated from the decay law which obeys Lin's theory were found equal for both 25 and 50 mesh lengths downstream of the grid (Table 2 and Table 3).

However, disagreements are seen to exist for the injection cases. The microscales shown in Table 3 increase steadily with injection rate at 25 mesh lengths and remain fairly constant at 50 mesh lengths downstream. For the cases of injection the Re_{λ_g} values as calculated from energy measurements and as calculated from the decay laws were found to be unequal (Tables 1, 2 and 3). It is seen that Re_{λ_g} calculated from energy spectrum measurements increase in a faster rate with increasing injection rate than the rate of increase of Re_{λ_g} calculated from the decay laws. Compared to the zero injection rate case, Re_{λ_g} was found to be 5 times as

large for the maximum injection rates case calculated from energy

spectrum measurement at 25 mesh lengths downstream of the grid.

The value is not too large, but seems sufficient already to show

the inertial subrange with this injection rate.

The increase of microscales with time at each injection rate

is due to the diffusive nature of the turbulent motion. It is

seen in Figure 14 that the energy generally decays according to

some negative power law approaching zero asymptotically. Mathe-

matically, it can be shown that the dissipation decreases accordingly

to a power law with a power one order of magnitude smaller than

the energy decay power. This means the dissipation is always

decreasing at a smaller rate than the turbulence energy.

The microscales obtained from energy spectrum measurements

were also found to increase faster with injection rate than the

increase of the microscales deduced from the decay laws. The rate

of increase of microscale with time is roughly represented by the

ratio of the microscale at 50 mesh lengths downstream of the grid

to the microscale at 25 mesh lengths. Again differences were

found between the result obtained from Lin and Karman-Howarth decay

laws and from spectrum measurements. The microscales and their

ratios are shown in Figures 24, 25 and 26. The ratio obtained

from spectrum measurements is generally smaller than that deduced

from the two decay laws.

In general, the disagreements are larger for higher injection

rates. This indicates that the turbulent flow generated by

the grid injection system is either non-homogeneous or it is of

an altered character which is still not well understood.

CHAPTER VI

CONCLUSIONS

As mentioned by Luxenberg in his thesis, a direct comparison of the characteristics of the turbulence generated by this grid injection system to that of homogeneous turbulence is not entirely possible due to the turbulence generating process of the grid, and unless the flow can be assured as sufficiently homogeneous. However, the results obtained from the present experiment could serve as description of the characteristics of the grid-injection turbulent flows.

First, the turbulence Reynolds number is increased by the injection of air into the main stream for all measurements. This is one of the advantages found with this mechanism. The Reynolds number, $Re_{\lambda g}$, was increased five times by injection while the grid mesh Reynolds number remains constant. The highest value of $Re_{\lambda g}$, obtained at the highest injection rate, is not so high as the minimum value of 1500 obtained by Stewart and Townsend for the inertial subrange. But the inertial subrange in this experiment was clearly distinguishable at about $Re_{\lambda g} = 100$.

The results obtained from pure grid turbulence (zero injection) measurements showed excellent agreements with the homogeneous tubulence theory. From the energy decay measurements, the results were found to follow Kolomogoroff's -10/7 power law with the assumption of Loitsiansky's invariant and self-preservation of the energy spectrum. In addition, the results were found to follow Lin's theory only by posing the assumption of partial similarity,

29

The results were also confirmed by the excellent agreement between microscale values obtained from energy spectrum measurements and Lin's decay law.

In the cases when air is injected, discrepancies occurred between the results obtained from energy spectrum measurements and Lin's decay law. According to the general power law, the decay in the highest injection case is found to follow a power dependence of 3.38 which is much higher than the value for homogeneous turbulence. obtained by other people and the value obtained in the present experiments with no injection. Although the result of energy decay agrees with Lin's decay law, disagreement was found between results deduced from both decay laws and results from the spectrum measurements. The rate of increase of microscales during decay for each injection rate is found to be smaller than that from the previous results. And the actual microscales are seen to be much larger for injection cases than that deduced from the decay laws.

This discrepancy is rather surprising because the spectra at 25 and 50 mesh lengths are clearly seen to decay with self-preservation or similarity for all injection rates. Also, with respect to energy decay, it seems to generally follow the decay laws. However, a judgment on the theory is not completely possible due to the lack of certainty with respect to the homogeneity and the lack of knowledge of the characteristics of the

turbulent flow generated by the grid injection system, although big improvement has been made.

The results obtained indicate that this type of turbulent flow does not exactly follow the laws of homogeneous turbulence. While injection is applied, the turbulence energy is increased when injection rate is increased. The microscales in the flow were found to increase more slowly with increasing injection rate than the value obtained from homogeneous turbulence decay laws. The rate of increase of microscale during decay is roughly represented by the ratio of microscales at 50 mesh lengths to that at 25 mesh lengths. Also, this ratio obtained from spectrum measurements is generally smaller than that deduced from the decay laws.

The results of this experiment, although confined by the turbulence generating device and its performance, have revealed some interesting characteristics of the turbulence generated by the combination of grid and air injection mechanism. The results also have confirmed the idea of increasing turbulence energy without increasing the size of the generating device and the velocity of the flow field. For further study, injection of air toward the upstream direction and against the upstream flow is expected to provide more uniform velocity and reasonable homogeneous conditions are expected to be obtained at downstream positions even closer to the grid.

APPENDIX A

BRIEF REVIEW OF TURBULENCE THEORY

The dynamics of isotropic turbulence (Ref. 8) is governed by the Navier-Stokes equations of motion

$$\frac{\partial u_i}{\partial t} + u_j \frac{\partial u_i}{\partial x_j} = - \frac{1}{\rho} \frac{\partial P}{\partial x_i} + \nu \Delta u_i$$

where u_i is the i direction component of the fluctuating velocity. For incompressible fluid, the equation was expressed in correlation form by Von Karman and Howarth (Ref. 7) as

$$\frac{\partial}{\partial t}(\overline{u_i^2} F) - \overline{u_i^2}^3 \left(\frac{\partial K}{\partial r'} + \frac{4}{r'} K \right)$$
$$= 2\nu \overline{u_i^2} \frac{1}{r'} \frac{\partial}{\partial r'} \left[\frac{1}{r'^2} \frac{\partial}{\partial r'} (r'^3 F) \right]$$

Using the Karman-Howarth equation, Taylor (Ref. 8) and Hinze (Ref. 7) showed the energy equation as

$$\frac{d \overline{u_i^2}}{dt} = - 10 \nu \frac{\overline{u_i^2}}{\lambda_g^2} \qquad (1)$$

which essentially gives the rate of decrease of kinetic energy.

Since the microscale λ_g is also a function of time, a specific description of the turbulent motion cannot be described without auxiliary assumptions.

To solve Eq. (1), several considerations were made by different persons. Von Karman and Howarth had first introduced the idea of

self-preservation of correlation functions. In terms of spectral language, this states that the spectrum remains similar in the course of time. Since the energy distribution among the various frequencies is changing through the transfer mechanism, this may be reasonably expected provided that there is enough time for the necessary adjustment.

Dryden (Ref. 7) based on the assumption of self-preservation had deduced the relation $\overline{u^2} \sim t^{-1}$. In his treatment, Loitsiansky's theory was not satisfied. But it has been known that Loitsiansky's invariant does exist although it is only true for a restricted type of isotropic turbulence and at very low Reynolds numbers.

A general decay law was suggested by Von Karman and Howarth based on the consideration that both Loitsiansky's invariance and self-preservation exist. _The decay law obtained is as

$$\overline{u^2} = c\, t^{-n}$$

or

$$\frac{\overline{u^2}}{\overline{U^2}} = c'\left(\frac{x}{M} - \frac{x_0}{M}\right)^{-n}$$

$$\lambda_g^2 = \frac{10}{n}\nu t$$

where n could be any constant. Kolmogoroff has further pointed out that the power law should be

$$\overline{u^2} = c\, t^{-10/7} \qquad\qquad \lambda_g^2 = 7\nu t$$

when Loitsiansky's invariant is true.

Another assumption that similarity of the energy spectrum

is occurring in eddies contributing appreciably to the dissipation

process and that the largest eddies play no role in determining

the similarity of the spectrum was considered by Lin (Ref. 7).

Upon the assumption that the decay of the total energy is deter-

mined predominantly by that of the energy containing eddies, the

additional relation $\dfrac{\mathcal{E}t^2}{\nu}$ = constant was introduced. The decay

law obtained by him is in the form

$$\overline{u^2} = a\left(t - t_o\right)^{-1} + b$$

or

$$\frac{\overline{u^2}}{\overline{U^2}} = a'\left(\frac{x}{M} - \frac{x_o}{M}\right)^{-1} + b'$$

$$\lambda^2 = 10\nu\left(t - t_o\right)\left[1 + \frac{b}{a}\left(t - t_o\right)\right]$$

where a and b are constants, and $a > 0$. This approach is

independent of Loitsiansky's invariant.

The assumption that the decay of the total turbulence is

determined mainly by the decay of the energy containing eddies has

obtained some support from experimental evidence given by

Betchelor (Ref. 9).

Another consideration was taken recently by Saffman (Ref. 10).

It has been known that Loitsiansky's integral is in general diver-

gent and that it is only for a restricted type of isotropic tur-

bulence that the Loitsiansky integral exists. But another invariant

was found by Saffman, namely

$$\int_o^\infty r'^2 R(r') \, dr' = C$$

where
$$R(r') = \frac{1}{8 \pi r'^2} \int_{|\vec{r}'|=r'} R_{ii}(\vec{r}') \, dA(\vec{r}')$$

$R_{ij}(\vec{r}')$ is the velocity covariance tensor and $dA(\vec{r}')$ is the element of area on a sphere of radius r'. The decay law which results from Saffman's invariant is

$$\overline{u^2} = C' t^{-6/5}$$

In his consideration, the turbulence is not necessarily isotropic, but the assumption of self-similarity is crucial.

The energy spectrum is defined by $E(\vec{k})$ such that

$$\overline{u^2} = \int_o^\infty E(\vec{k}) \, d\vec{k}$$

where $E(\vec{k})$ represents the contribution to the mean square of the total signal of the turbulence component with the wave number $\vec{k}$ in the wave number space. The related one dimensional spectrum in time-frequency space is

$$\overline{u_i^2} = \int_o^\infty E_i(f) \, df$$

where $E_i(f)$ is the contribution at frequency f.

Theories of the spectrum have shown that the decay of the larger eddies occurs at a slower rate at low wave number range than the total decay of turbulence energy. The smaller eddies have a shorter characteristic time compared with total time of decay, namely, decay at a faster rate.

During the decay, energy is transferred from large size eddies to smaller size eddies, then again to ever smaller ones and finally, at some small size eddies, the energy will be dissipated into heat. Kolmogoroff has considered this process and given the name equili-brium range to the portion of high wave number range where the spectrum is statistically independent of the formation of the turbulence. The dissipation in this range increases as the wave number increases. When the Reynolds number is sufficiently large, the dissipation in the region of wave number very far below the region of maximum dissipation will be negligibly small compared with the flux of energy transferred by inertial effects. It is thus called the inertial subrange.

For isotropic turbulence, the spectrum curve is in proportion with $-5/3$ power of k in the inertial subrange and with -7 power for very large values of k (ref. 8).

APPENDIX B

PERFORMANCE OF GRID WITH DIFFERENT HOLE DISTRIBUTIONS

As mentioned in Section 2-(2), the grid used by Conger and

Luxenberg (Ref. 7 and 10) was made to generate flows with uniform

velocity far downstream of the grid. One of the major tasks in the

present experiment was to modify the grid and to generate the uni-

form flow starting from positions very close to the grid (about 20

mesh length). However, this was found to be difficult because of

the lack of knowledge about the flows in the grid system. The

problem was solved by trial and error. Several hole size distri-

bution with different jet part configurations were tried. The

different performances of each grid will be discussed in the

following paragraphs.

A preliminary investigation of the performance of the original

grid was made to aid in the design task. The grid was made with

larger holes in the outer region near the wall in order to inject

larger momentum to compensate for boundary effects. Figures 27

and 28 give a picture of the velocity profiles between 20 orifice

diameter downstream to 82 mesh length downstream (end of test

section).

It is seen that up to 57 mesh length, the maximum velocity

occurs near the wall, and the velocity tends toward uniformity

toward the end of the test section.

It was decided that the easiest way to modify the grid was

to change the distribution of hole sizes. A grid with holes of

uniform size of 0.020 inch and with the same locations as before
(Ref. 8) was tried. Surprisingly, it was found that the velocity
profile still showed non-uniformity. Figure 29 shows the measure-
ments taken at 20 mesh lengths downstream. Several trails were then
made to overcome this defect.

First, a trial was made by increasing the four center holes to
a 0.022 inch diameter. Figure 30 shows the velocity profile obtained
with this hole distribution. It is seen that such a small increase
in injected momentum caused an overshoot in the center region. It
is also seen that there was no improvement to the large velocity
gradient at the region closer to the wall.

A second trial was then made using special tubes in the grid.
The wall thickness of the tubes, at the portion where the orifices
locate, was increased. This configuration was intended to give
the jets more directional guidance in order to eliminate the
momentum effect mentioned by Luxenberg (Appendix B in Reference 3).
The velocity profile obtained with this grid is shown in Figure 32.
It is seen that the deviation from uniformity of the velocity was
not improved by this method.

From the results obtained in the above two trials, it is seen
that the non-uniformity in velocity profiles obtained with the grid
with uniform hole size is not caused by the momentum effect,
although the pressure drop in the grid tubes is still a possible
cause. Therefore, an attempt was made to improve the hole distri-
bution to overcome the non-uniformity in velocity.

Considering the hole distribution shown in Figure 2 (original hole distribution), there are no jet ports near the wall. There are some portions on the grid where the spacing of the orifices from the wall is about the same as with neighboring orifices. No momentum is injected in the region near the wall. Therefore, holes were added in this region, as shown in Figure 3. The extra holes are of two different sizes in order to try to create a uniform distribution of injected momentum.

The velocity profiles obtained with the grid with the extra holes are shown in Figure 32. The deviation of velocity from the mean is reduced to less than 5 percent. Without the extra holes, the deviation is more than 10 percent as can be seen in Figure 29. The area of the uniform velocity region was increased from $\pi(0.4R)^2$ to $\pi(0.6R)^2$ as the extra holes were added, the increase is more than a factor of two.

A final point to be mentioned is that the accuracy of location of the orifices plays an important role in the uniformity of the velocity field. The orifices have to be located within 0.0005 inch laterally from the center of the tubes on the grid plane. Small off positioning causes the jets to become non-parallel and the momentum distribution non-uniform. As a consequence, the velocity field downstream would be non-uniform. An example is shown in Figure 33. It also was found to be very important to remove all burrs both inside and outside the tubes finally, by polishing with cloth.

APPENDIX C

ENERGY SPECTRUM NORMALIZATION

The energy spectra were normalized and non-dimensionalized

to $\dfrac{E_1}{\overline{u_1^2}\,\lambda_g}$ and the wave number space as $k\lambda_g$. The normalization

factor was calculated and integrated by the equation

$$\overline{u_1^2} = \int_0^\infty E_1(k)\,dk \qquad (C.1)$$

for isotropic turbulence.

The microscale parameter λ_g was obtained and is the equation

$$\frac{1}{\lambda_g^2} = \frac{2}{\lambda_f^2} = \frac{2\pi^2}{\overline{U^2}\,\overline{u_1^2}} \int_0^\infty f^2 E_1(f)\,df \qquad (C.2)$$

(Ref. [8]), where λ_g and λ_f are the lateral and longitudinal
measurements of microscale.

The integral in the right hand side in Eq. (C.2) is directly
integrated from the measurement E. Since $\overline{u_1^2}$ is also a direct
result from experimental measurements, it follows that λ_g is also
a direct result. This is important not only to the plotting of
energy spectra but also for the comparison of results with
theory and other experimental results. The results obtained are
discussed in Chapter V.

40

REFERENCES

1. Teunissen, H. W., "An Ejector-Driven Wind Tunnel for the Generation of Turbulent Flows with Arbitrary Mean Velocity Profile," UTIAS Technical Note No. 133.

2. Conger, W. L., "The Measurement of Concentration Fluctuations in Mixing of Two Gases by Hot Wire Anemometer Techniques," Univ. of Pennsylvania Dissertation, 1965.

3. Luxenberg, D. S., "Some. Effects. of. Air Injection on the Turbulence Generated by a Bi-Planar Grid," Case Western. Reserve. Univ., Master's Thesis, Department of. Fluid, Thermal & Aerospace Sciences, 1969.

4. King, L. V., "On the Convection of Heat from Small Cylinders in a Stream of Fluid," Phil. Trans. of. Roy. Sec., A214, 1914.

5. Instruction Manual, Model 50, Constant Current Hot Wire Anemometer System," Shapiro & Edwards Company.

6. Instruction Manual, Type 1900-A Wave Analyzer, General Radio Company.

7. Lin, C. C., Turbulent Flows and Heat Transfer, Vol. 5, Princeton Univ. Press, 1954.

8. Hinze, J. W., Turbulence, McGraw Hill, 1959.

9. Betchelor, G. K., Homogeneous Turbulence, Cambridge Univ. Press, 1960.

10. Saffman, P. G., "Note on Decay of Homogeneous Turbulence," Physics of. Fluids, Vol. 10, No. 6, June 1967.

11. Kovasznay, Leslie, S. G., "Turbulence Measurements," Physical Measurements in Gas Dynamics and Combination, Vol. 9 Princeton Univ. Press, 1954.

timing belt

fan section

smoothing section

grid manifold

ports for air injection

test section

contraction cone

inlet

motor

42
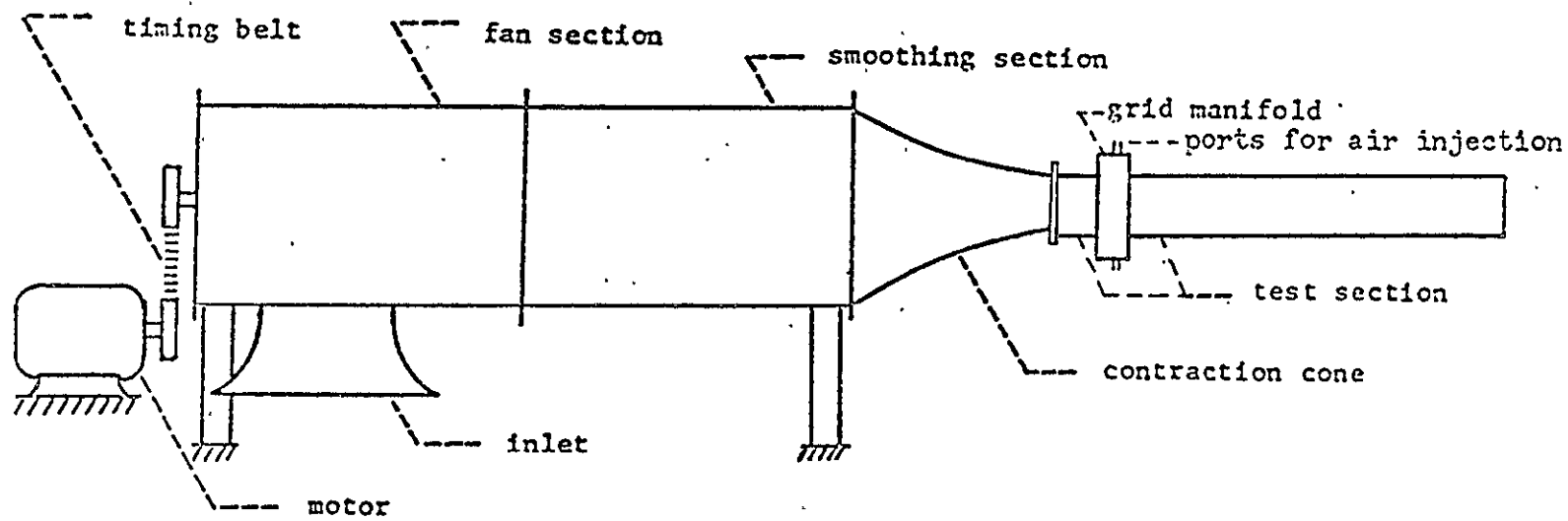
Figure 1   WIND TUNNEL AND TEST SECTION CONFIGURATION

18 Hollow Rods (5/32" O.D.,
1/32" wall thickness) in a
biplanar grid with Mesh 5/8".

Four inlect ports
are connected to
one manifold.

A

Matrix of 140
orifices (0.0135"
to 0.020").

A'

$5\frac{5"}{8}$
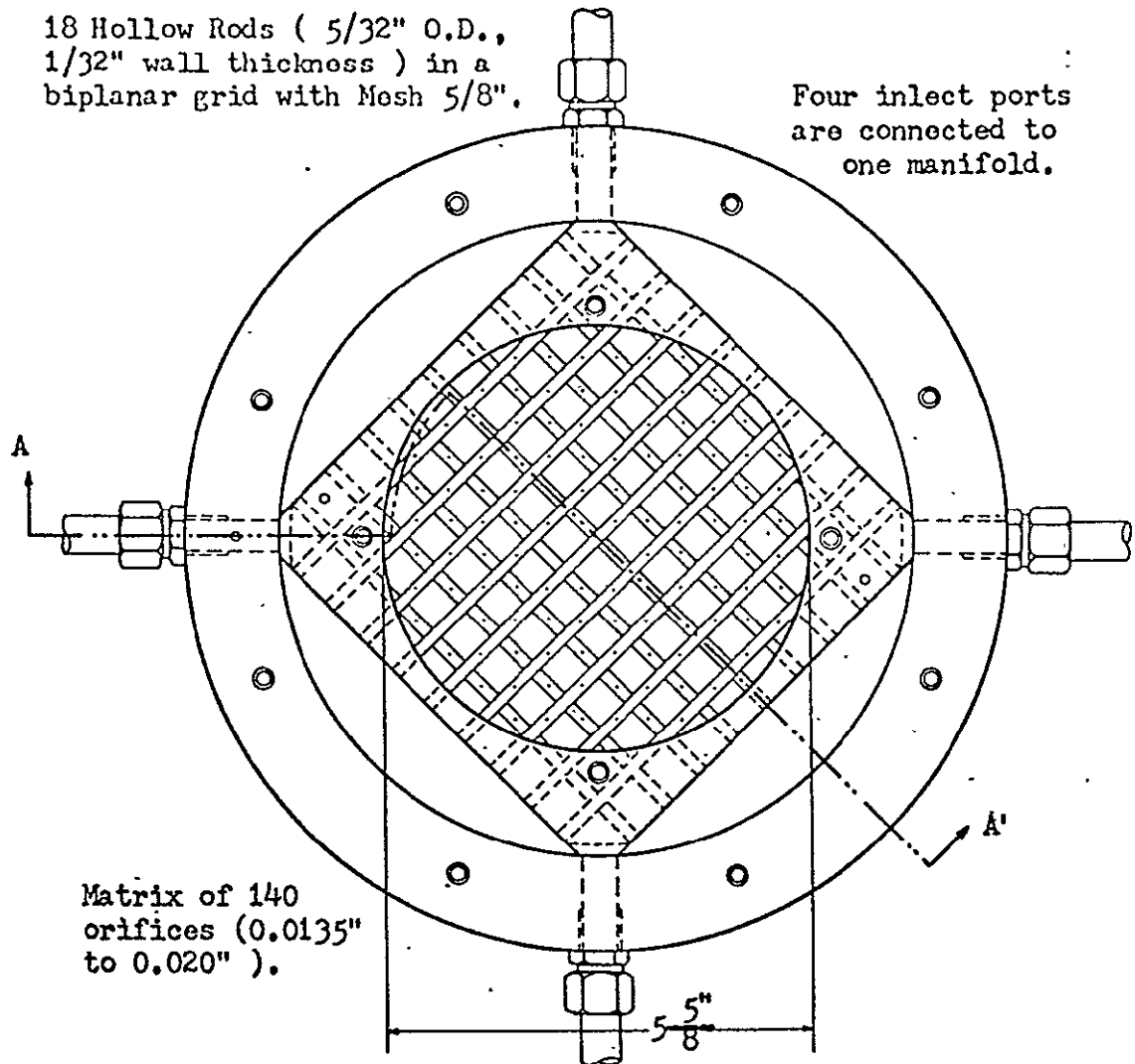
View With Cover Removed
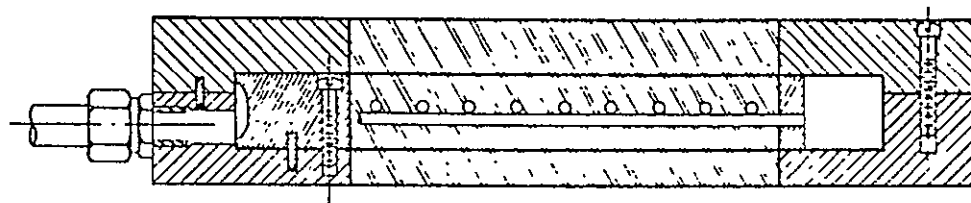
Section AA'

Figure 2   GRID – INJECTION DEVICE
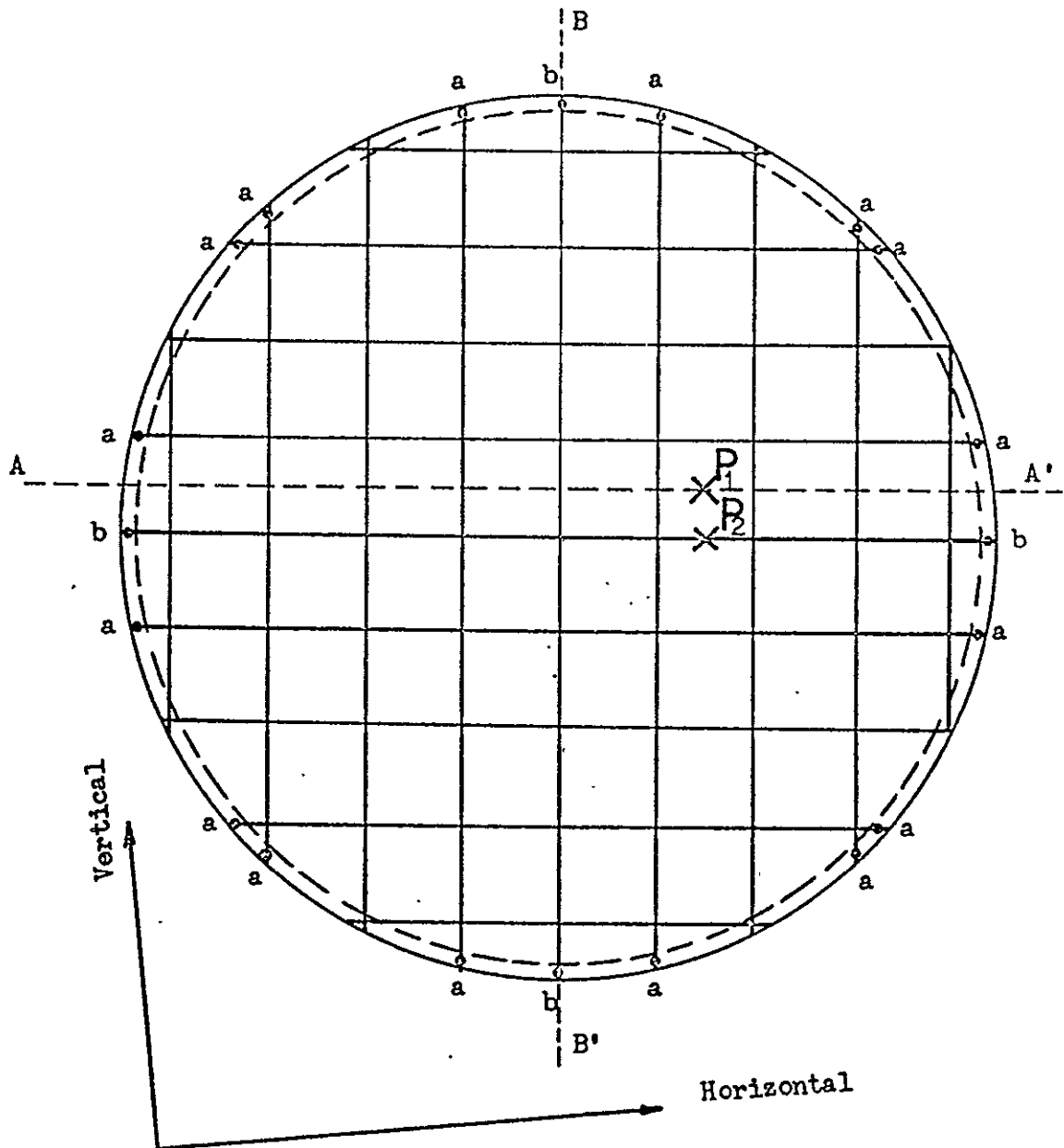
Holes inside of dotted circle: Uniform size of
0.020 inch, located
at the middle of each
side of mesh square.

Extra holes near the wall: a: 0.0135 inch
                                 b: 0.0160 inch

Figure 3   DISTRIBUTION OF HOLE SIZE IN GRID
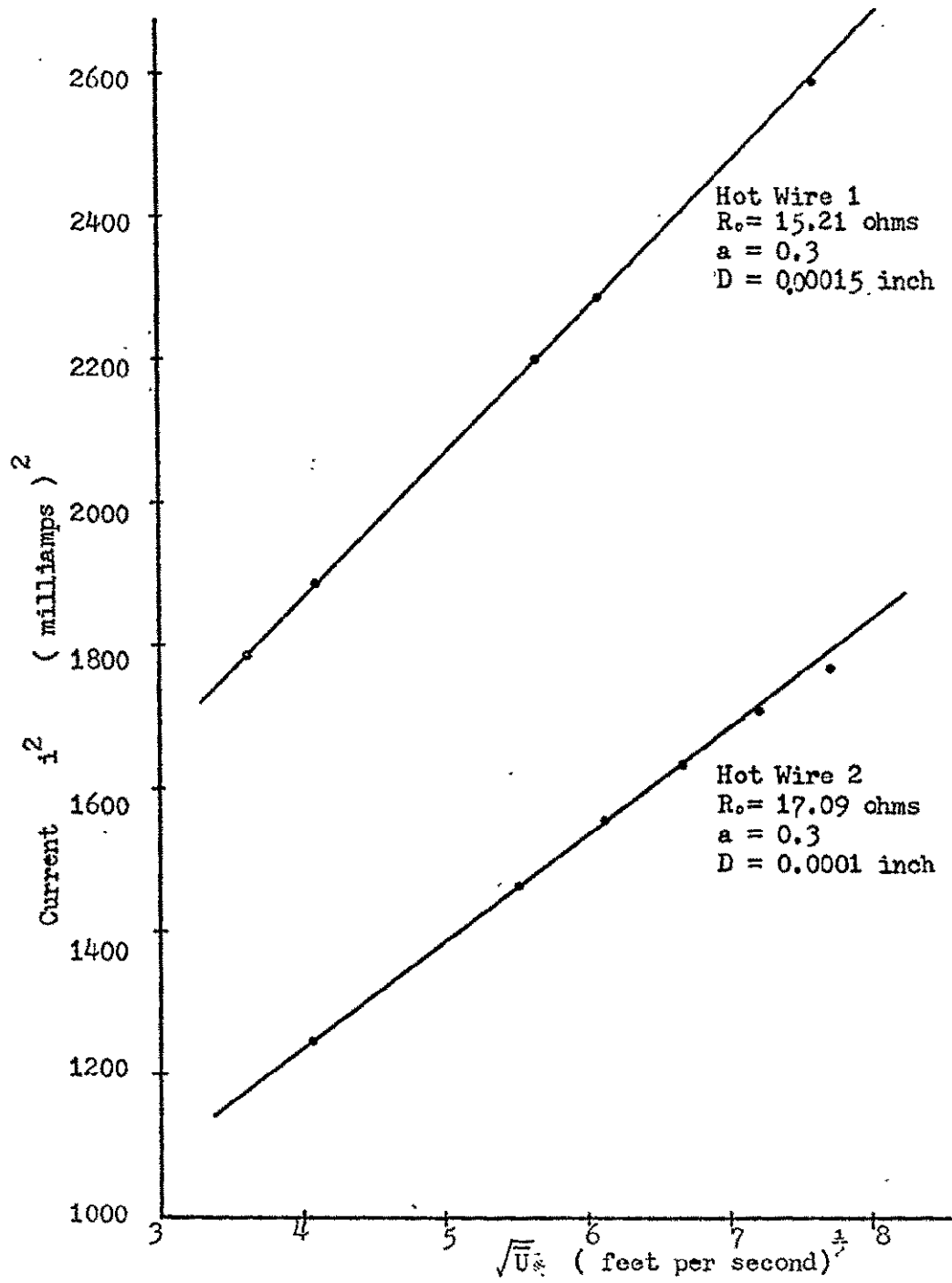
Figure 4   HOT WIRE CALIBRATION CURVES

$\dfrac{r}{R_u}$

IRP = 1.88

Horizontal Traverse
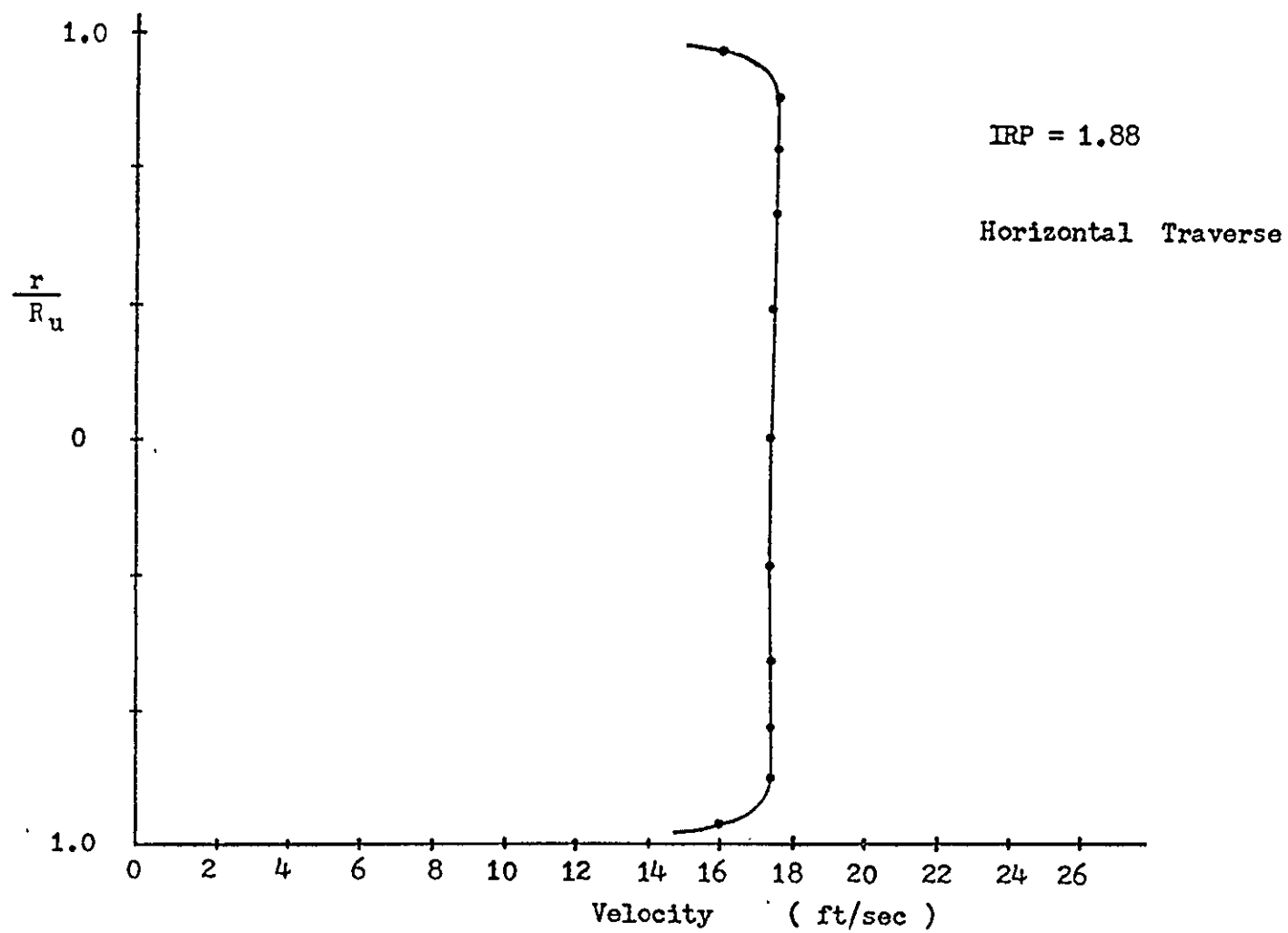
Velocity   (ft/sec)

Figure 5   VELOCITY PROFILE UPSTREAM OF GRID
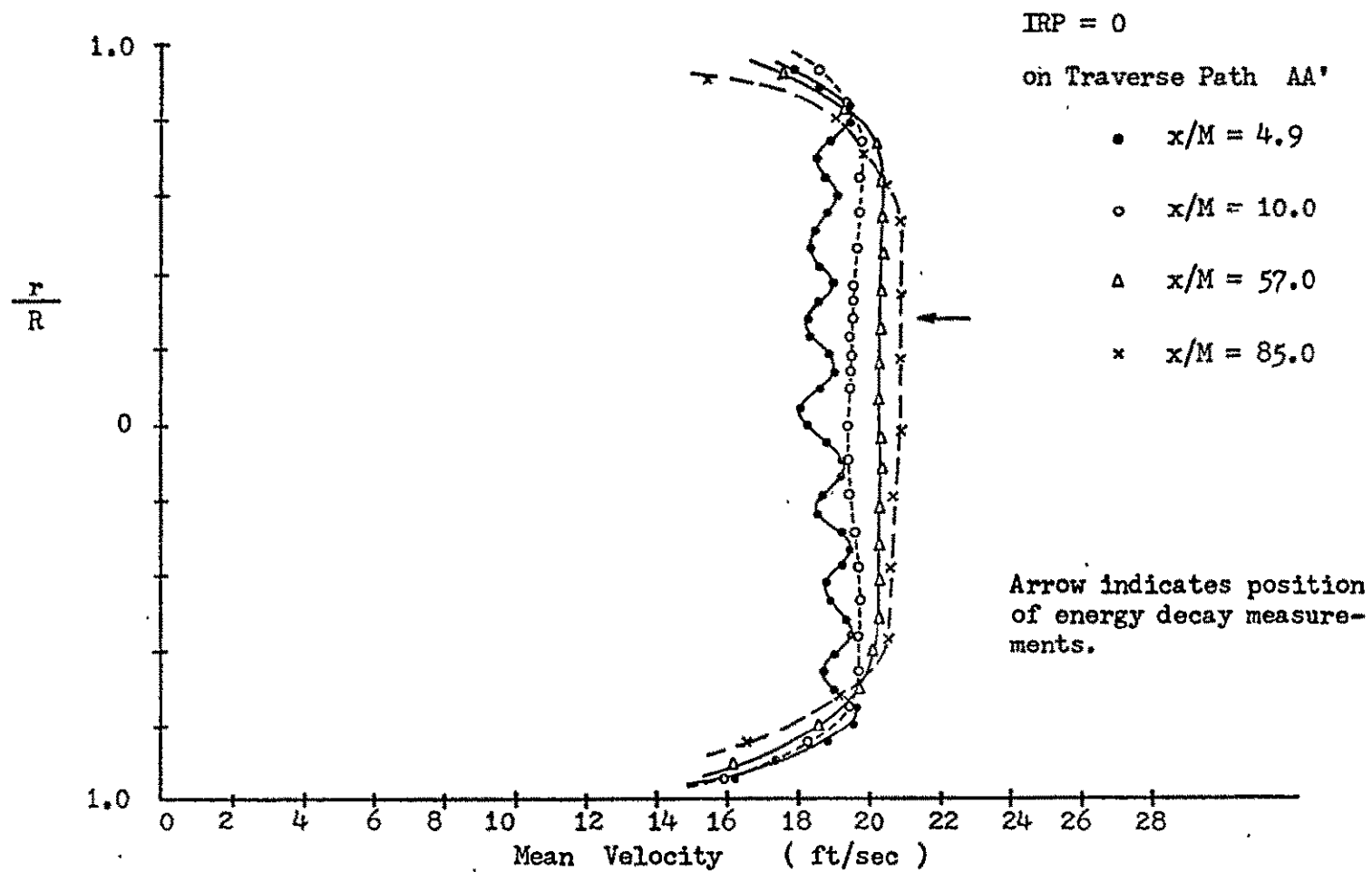
Figure 6   MEAN VELOCITY PROFILE

47

Figure 7   MEAN VELOCITY PROFILE ..
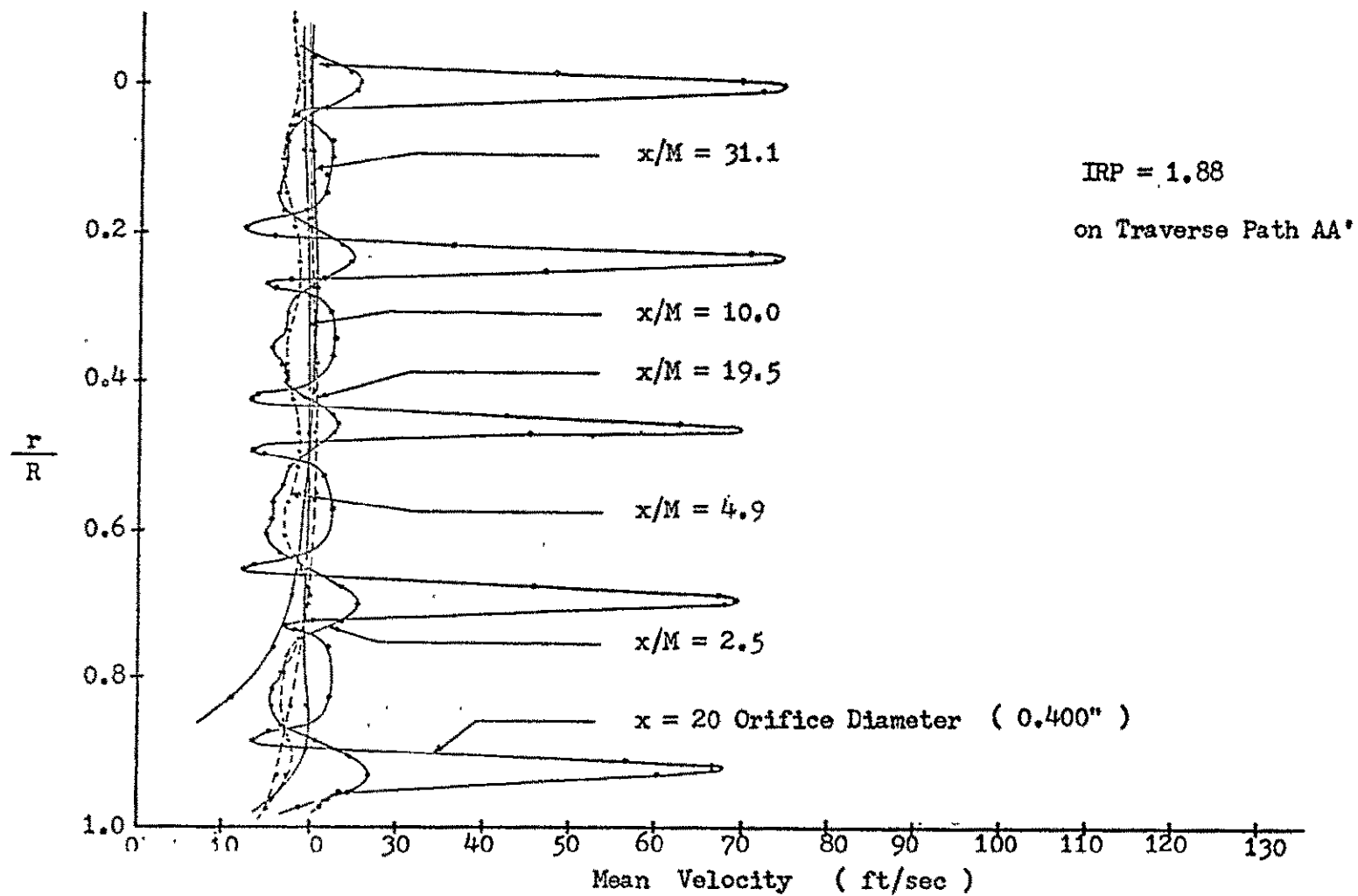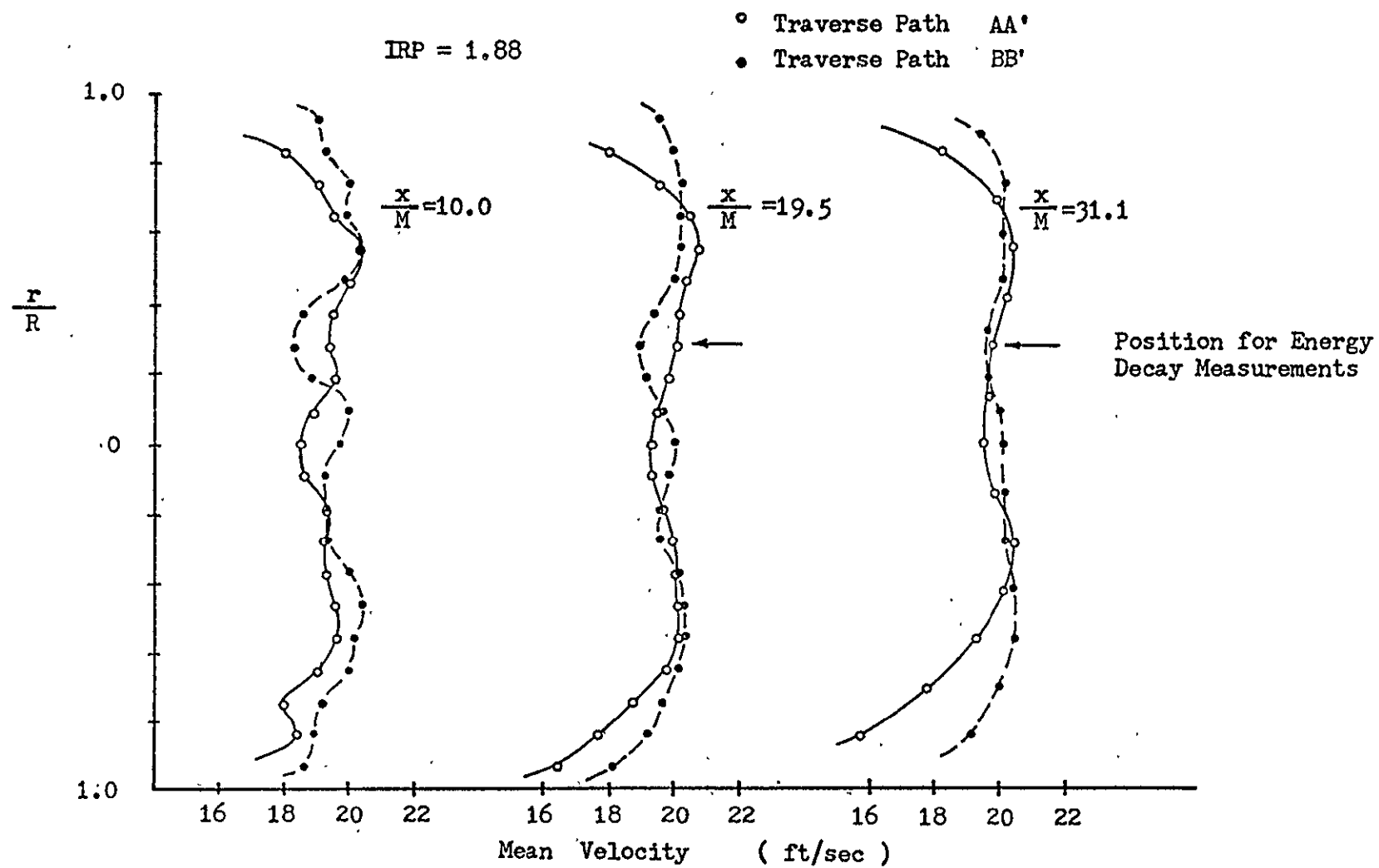
Figure - 8   MEAN VELOCITY PROFILE
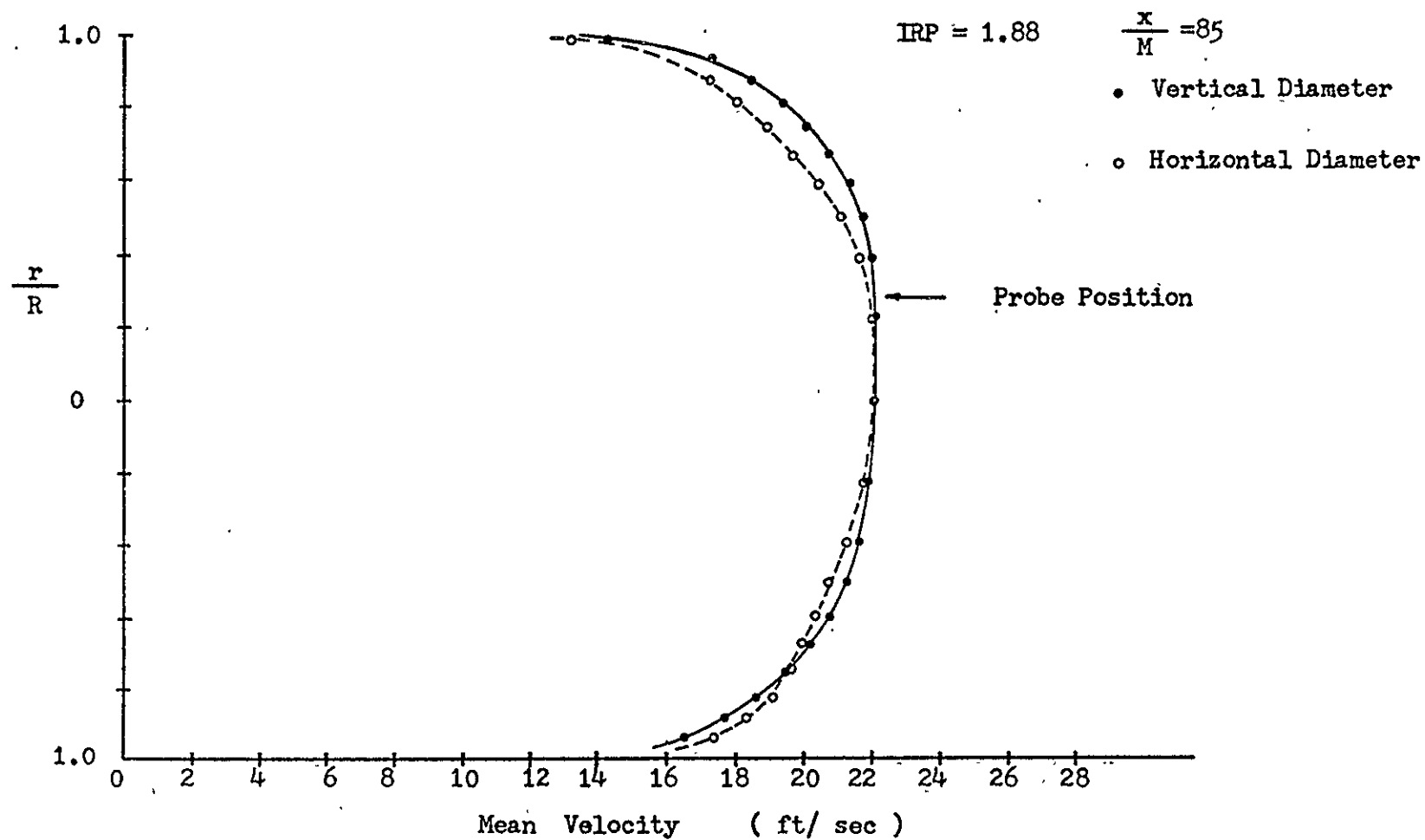
Figure 9 . MEAN VELOCITY PROFILE AT END OF TEST SECTION .
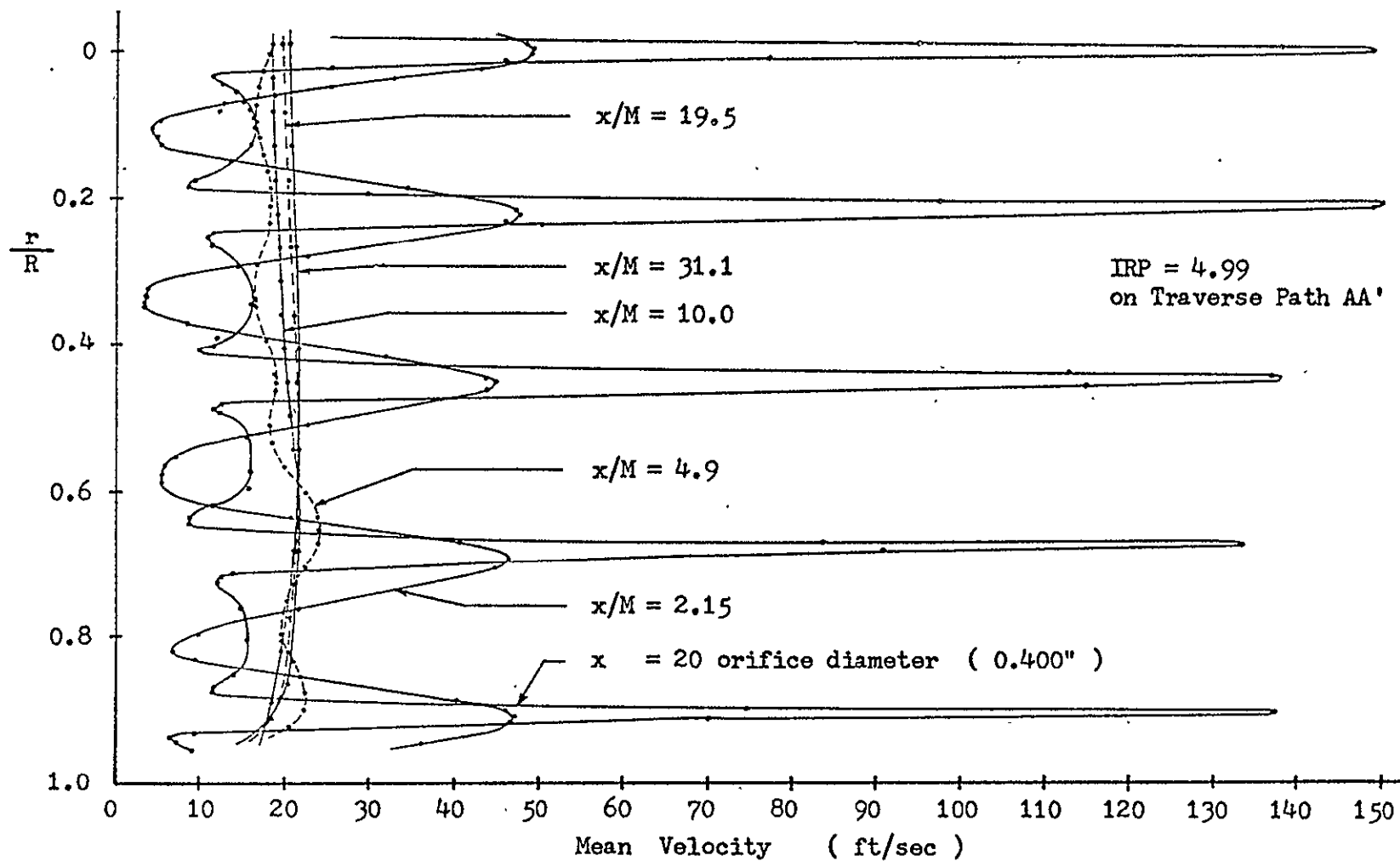
Figure 10   MEAN VELOCITY PROFILE
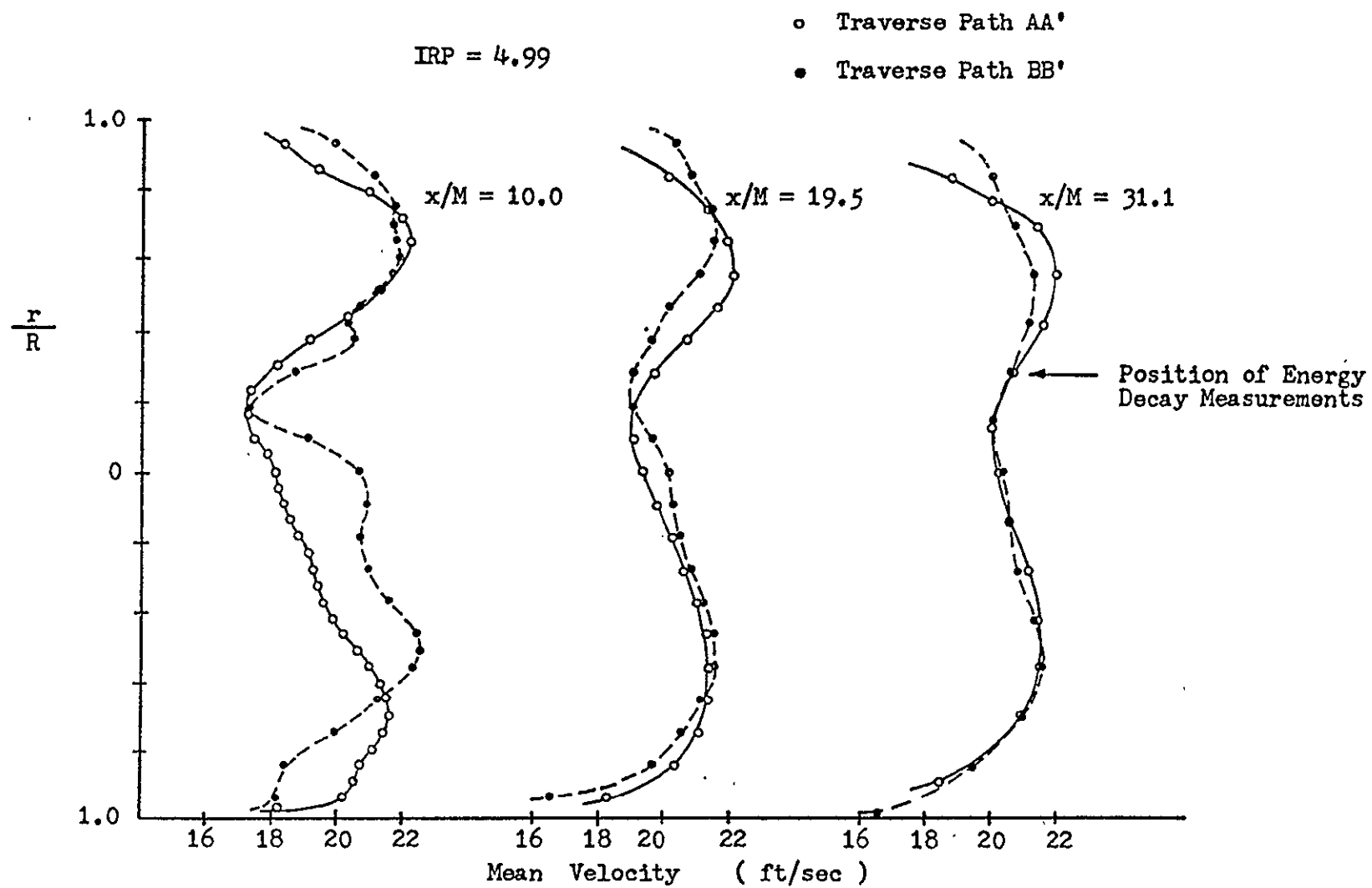
Figure 11   MEAN VELOCITY PROFILE
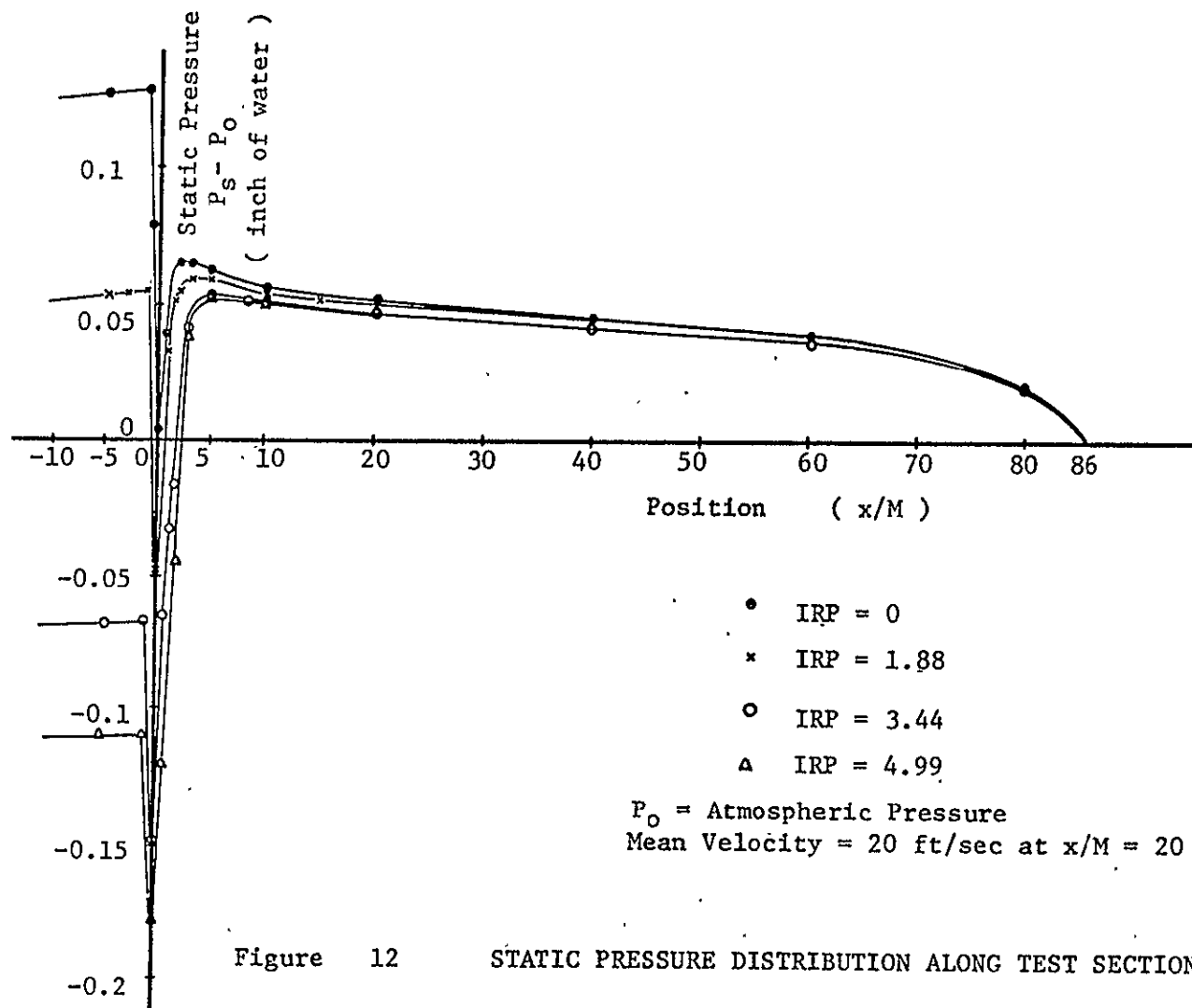
Figure   12   STATIC PRESSURE DISTRIBUTION ALONG TEST SECTION LENGTH

- IRP = 0
- × IRP = 1.88
- ○ IRP = 3.44
- △ IRP = 4.99

P_O = Atmospheric Pressure
Mean Velocity = 20 ft/sec at x/M = 20
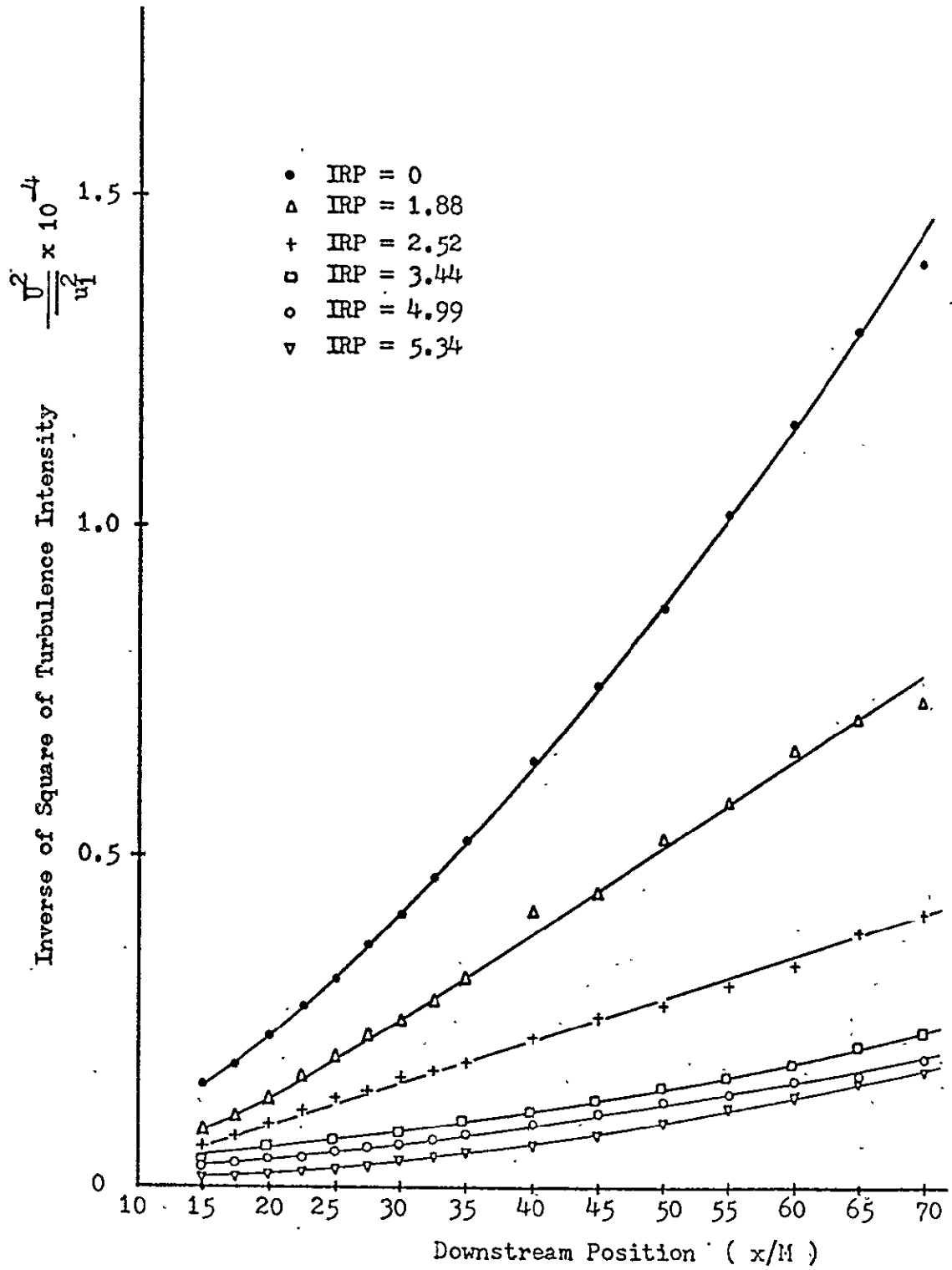
Figuro 13   TURBULENCE ENERGY DECAY WITH DOWNSTREAM POSITION
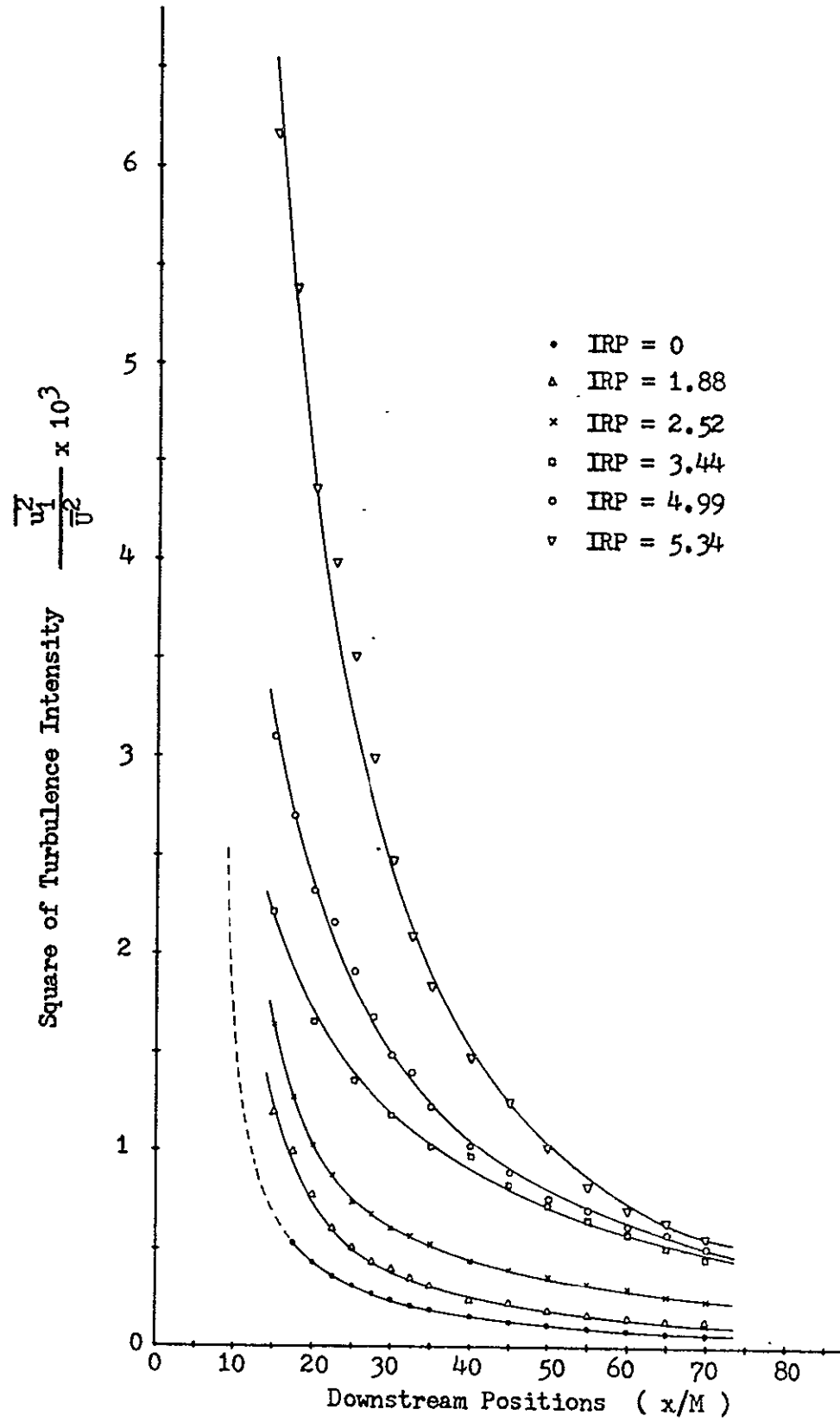
Figure 14   TURBULENCE ENERGY DECAY WITH DOWNSTREAM POSITION
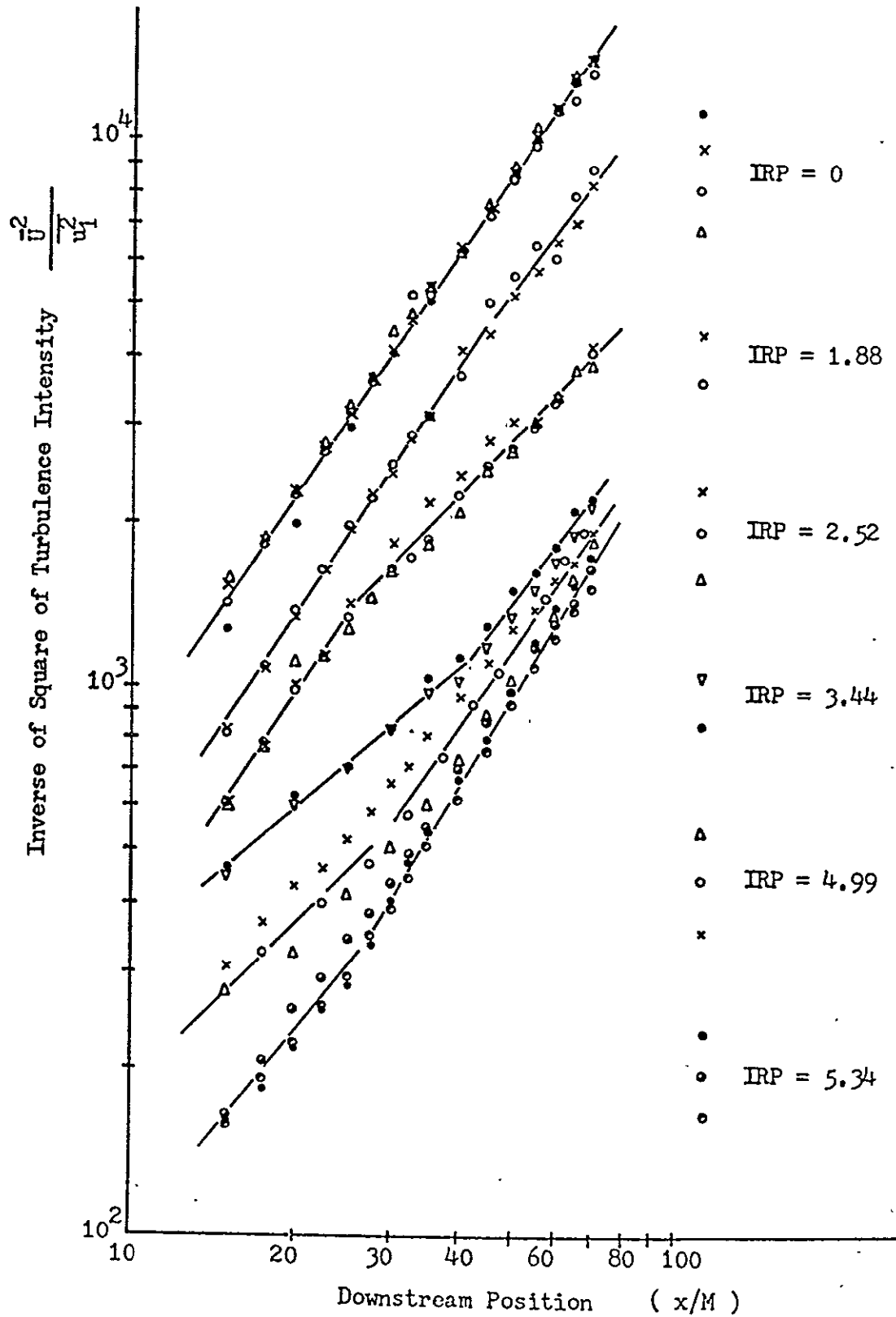
Figure 15   TURBULENCE ENERGY DECAY WITH DOWNSTREAM POSITION
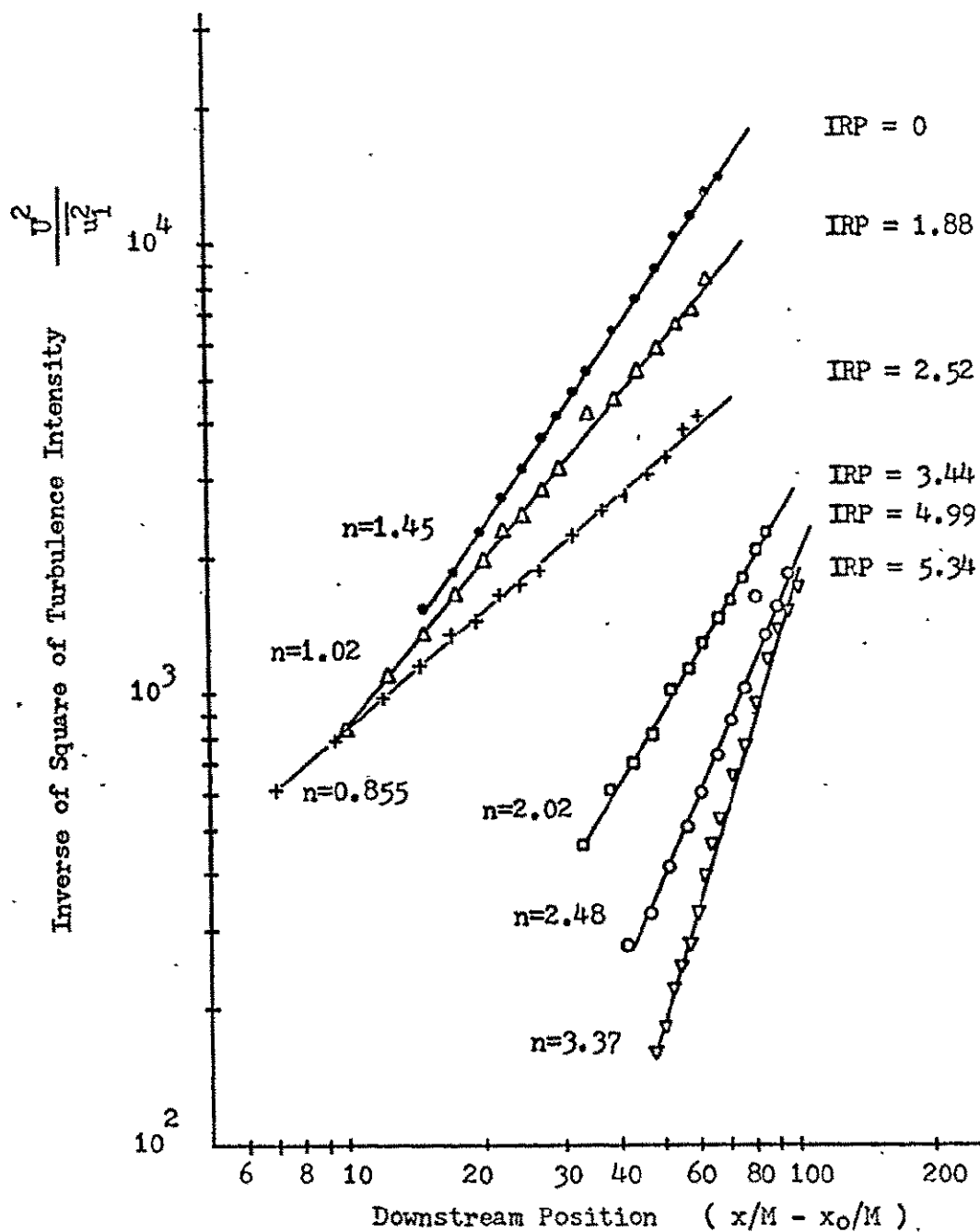
Figure 16   TURBULENCE ENERGY DECAY PLOTTED ACCORDING T(

$$\frac{\overline{u_1^2}}{\overline{U^2}} = c' \; (\; x/M - x_o/M \;)^{-n}$$
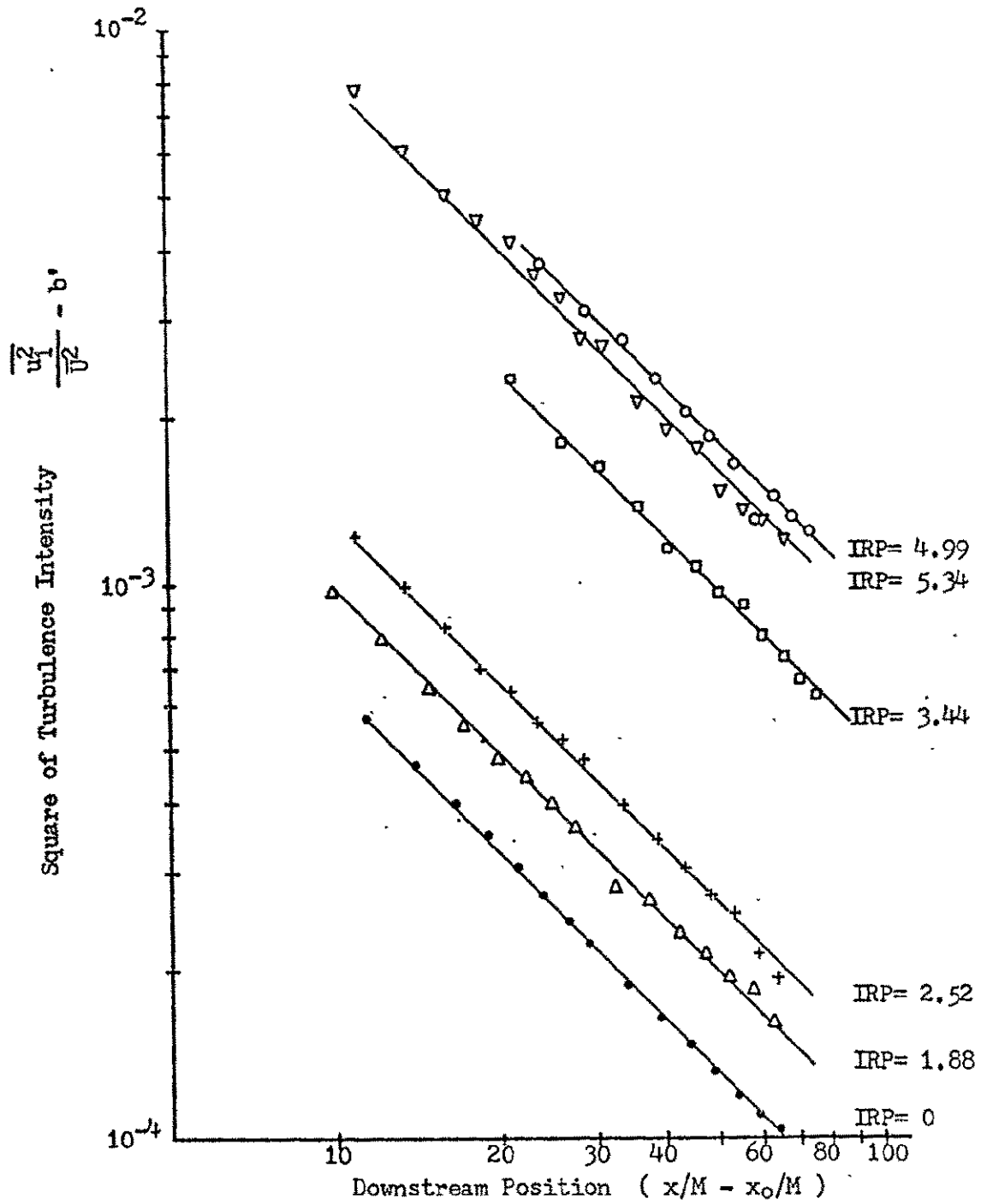
Figure 17   TURBULENCE ENERGY DECAY PLOTTED ACCORDING TO

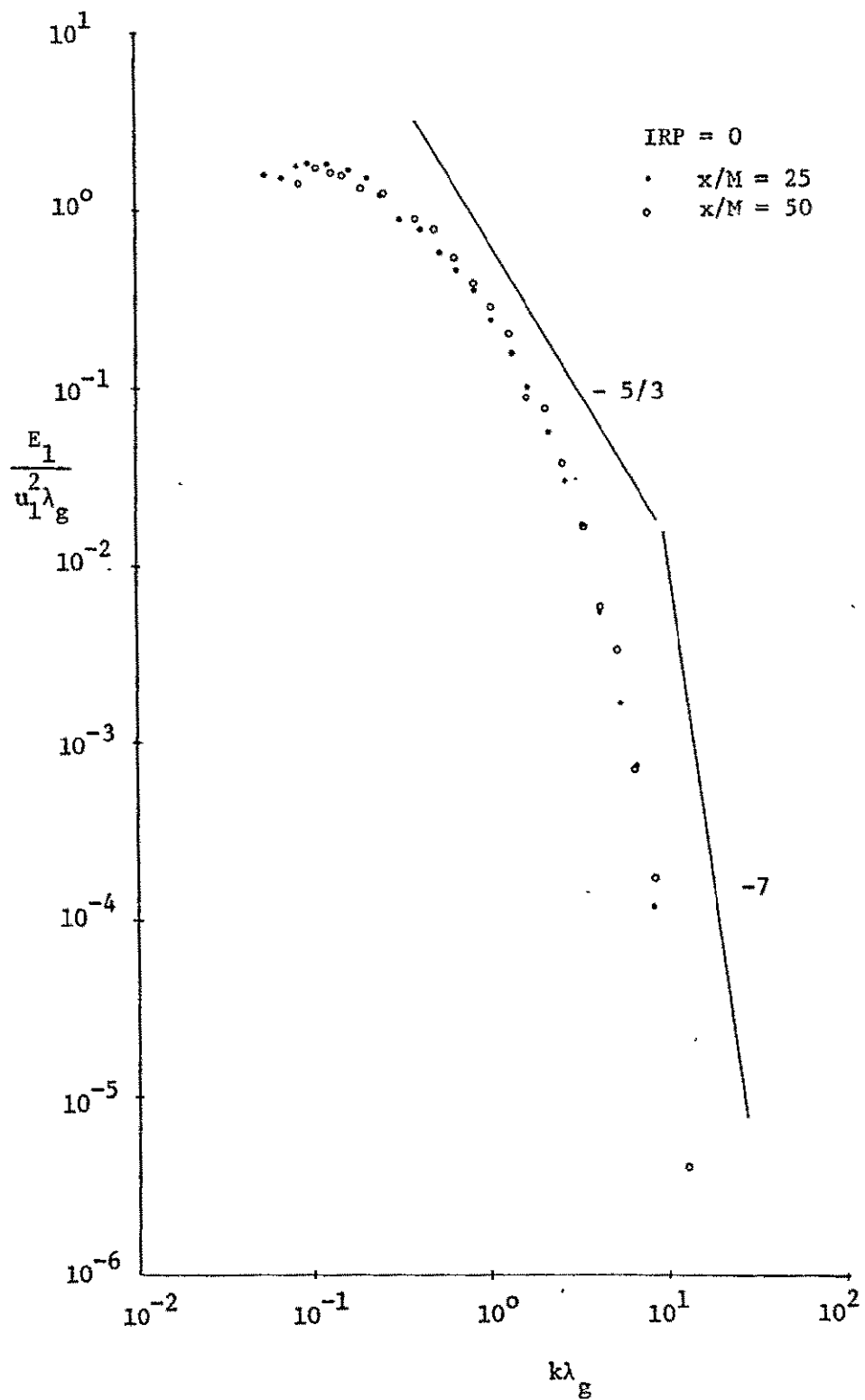$$\frac{\overline{u^2}}{U^2} = a'(\ x/M - x_o/M \ )^{-1} + b'$$

Figure 18   ENERGY SPECTRA
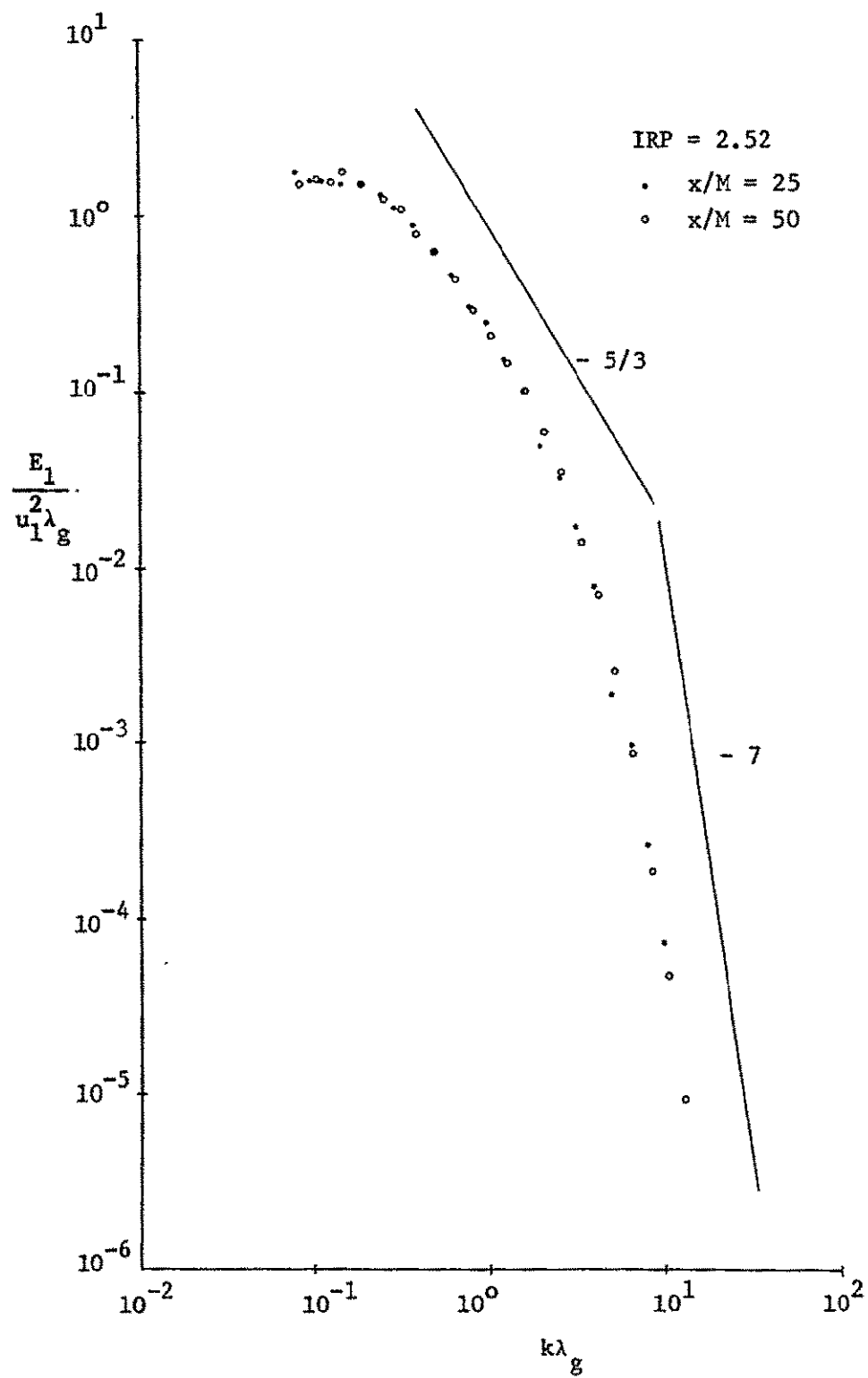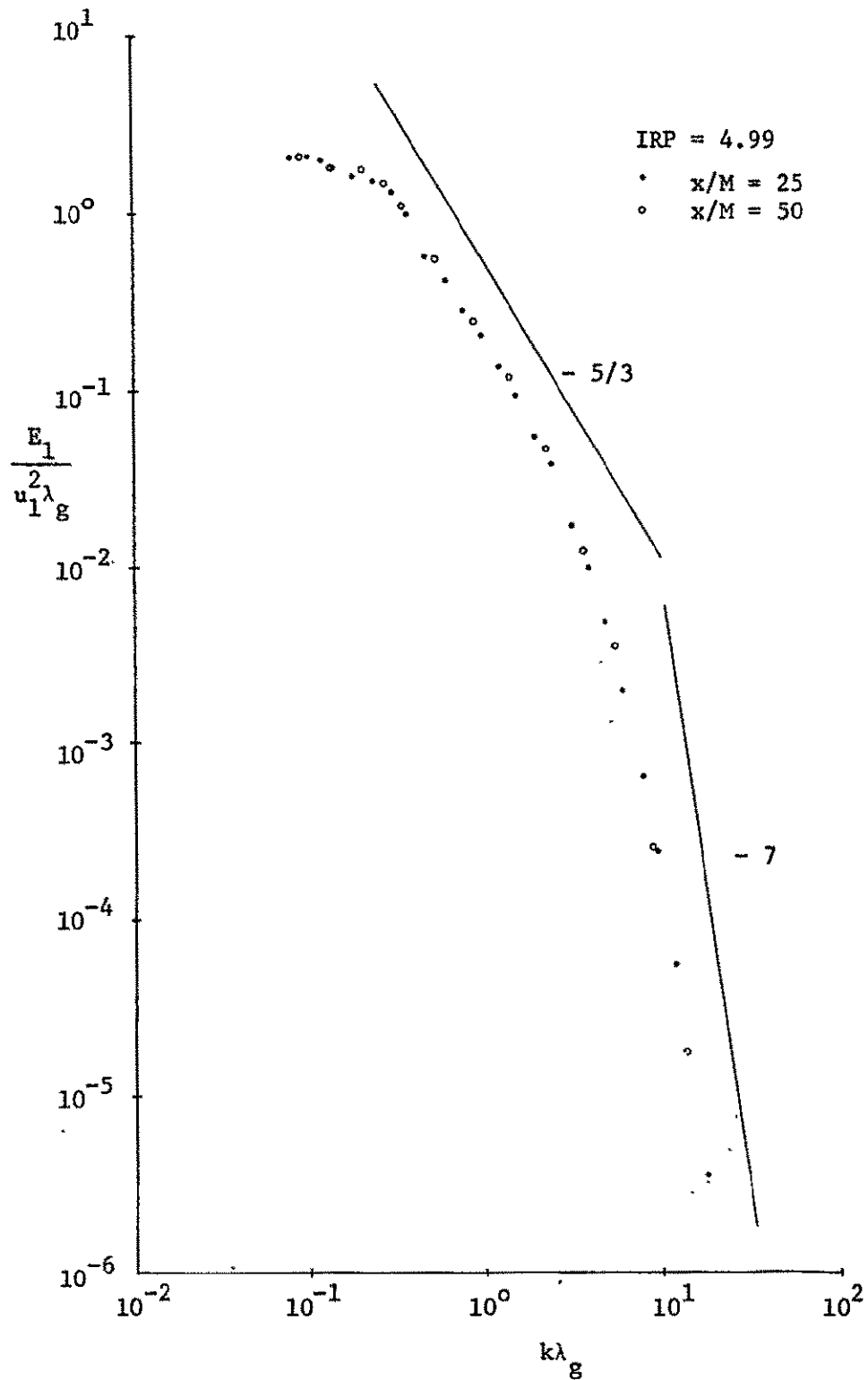
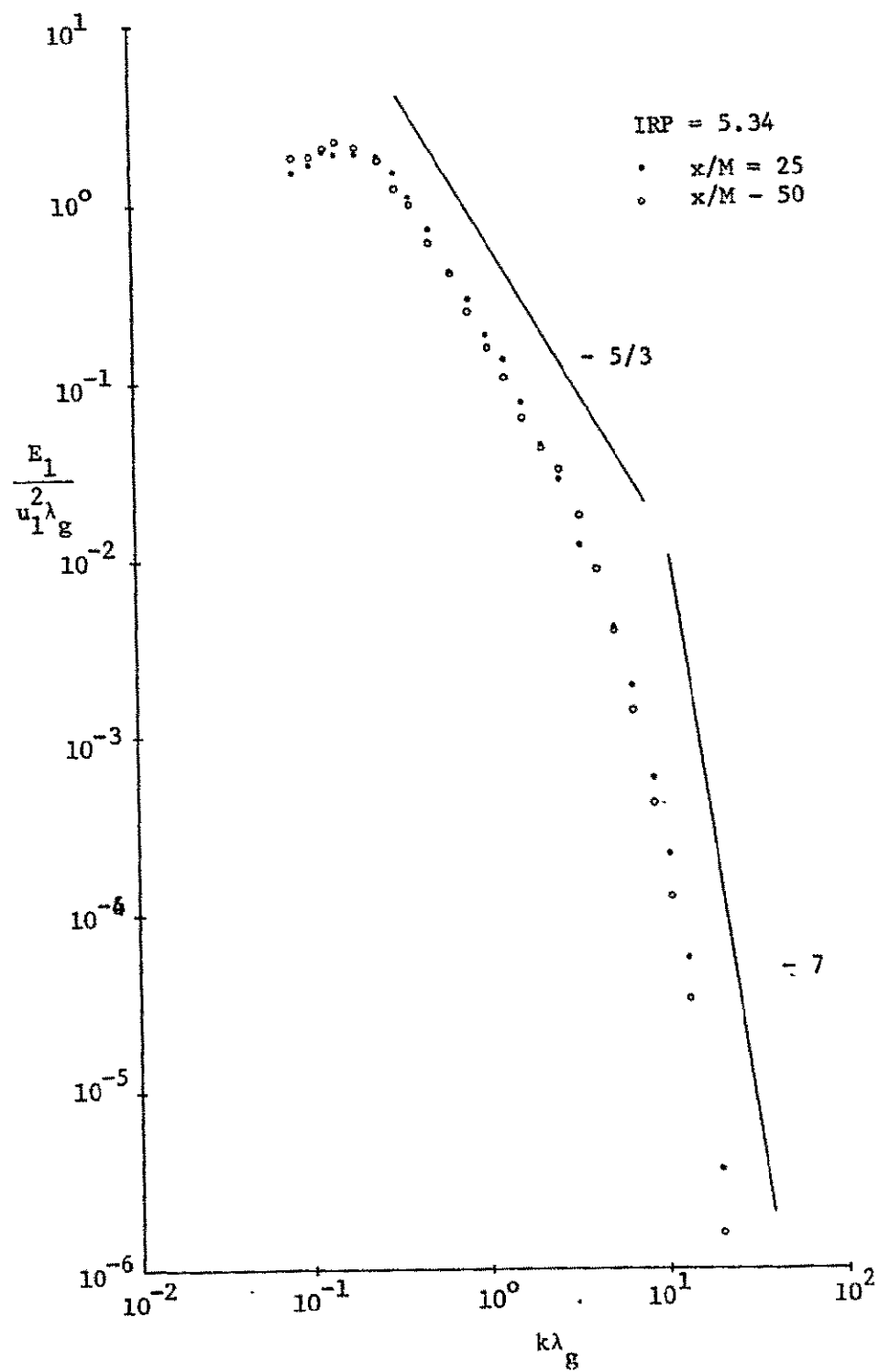Figure   19   ENERGY SPECTRA

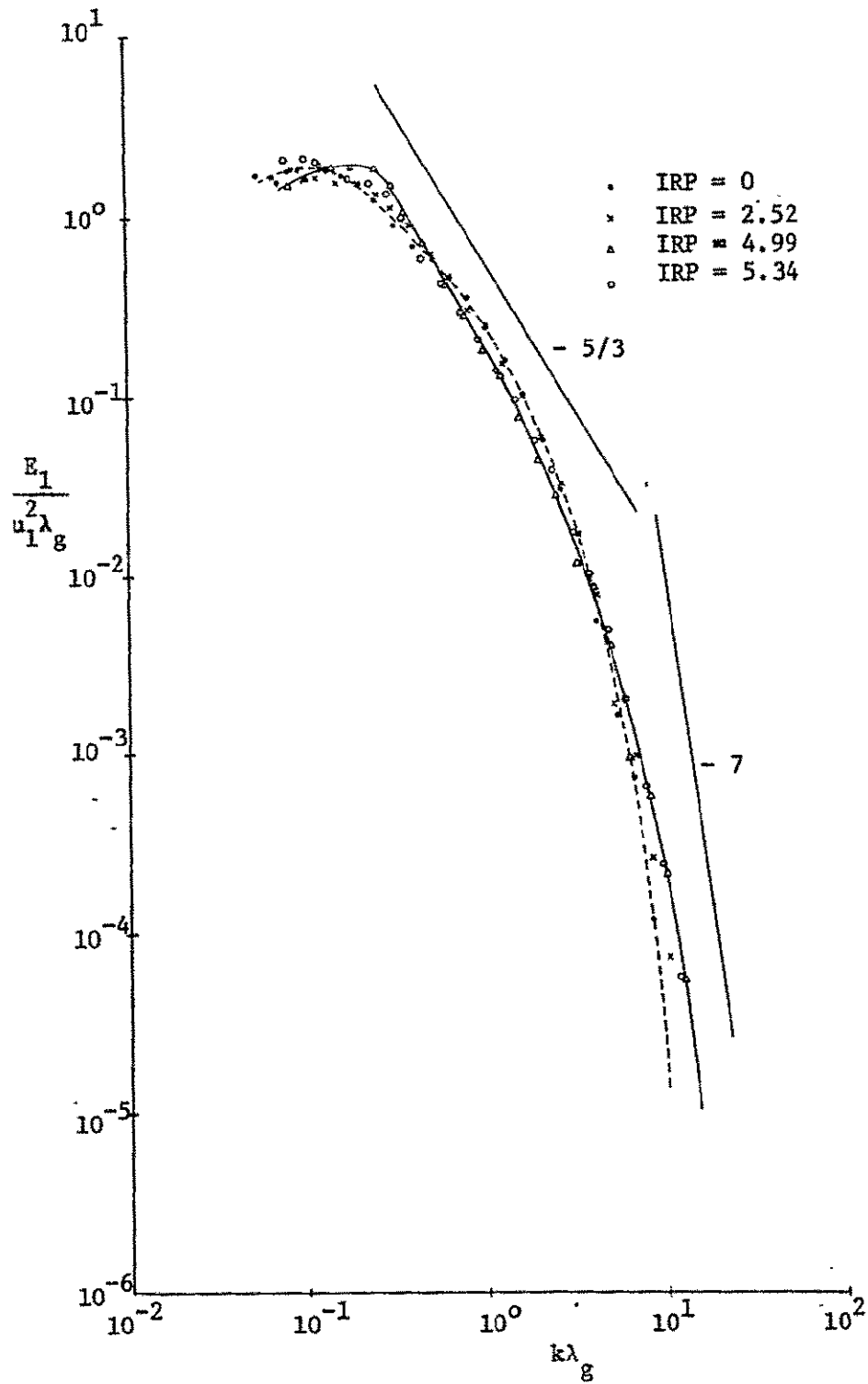Figure 20   ENERGY SPECTRA

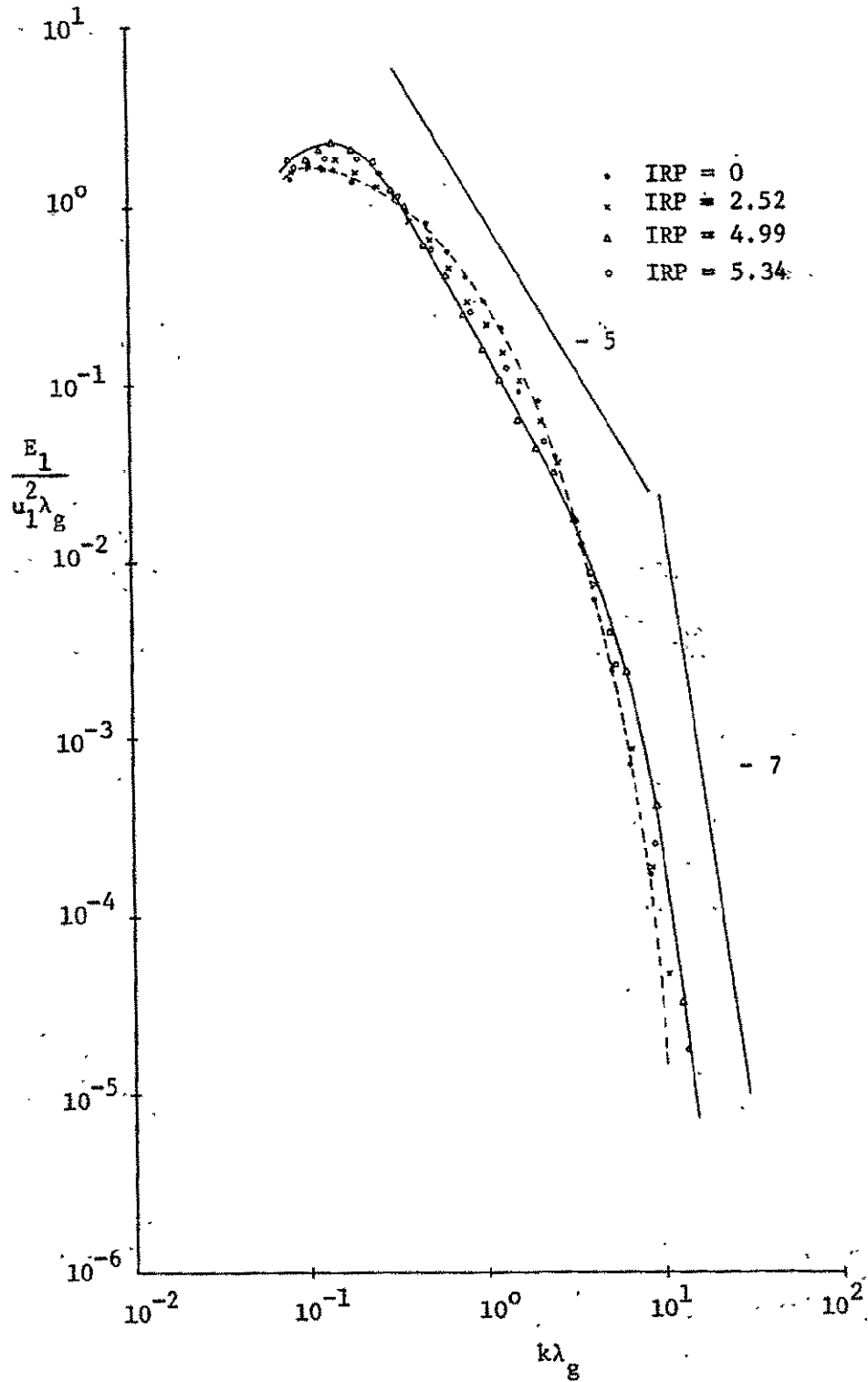Figure 21   ENERGY SPECTRA

Figure 22   ENERGY SPECTRA AT x/M = 25

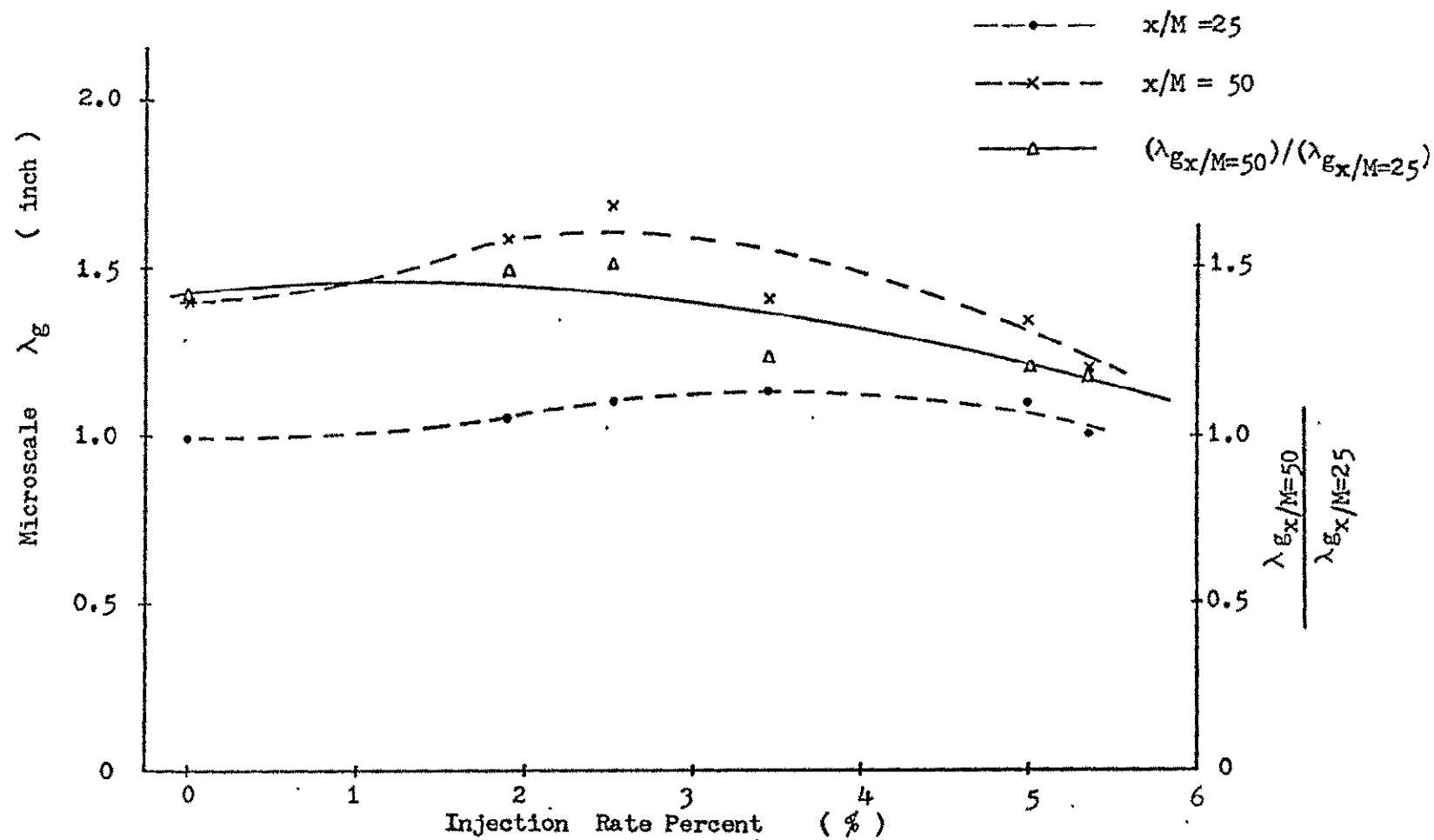Figure 23   ENERGY SPECTRA AT x/M = 50

Figure 24 MICROSCALES DEDUCED ACCORDING TO $\dfrac{\overline{u_1^2}}{\overline{U^2}} = c'(x/M - x_0/M)^{-n}$
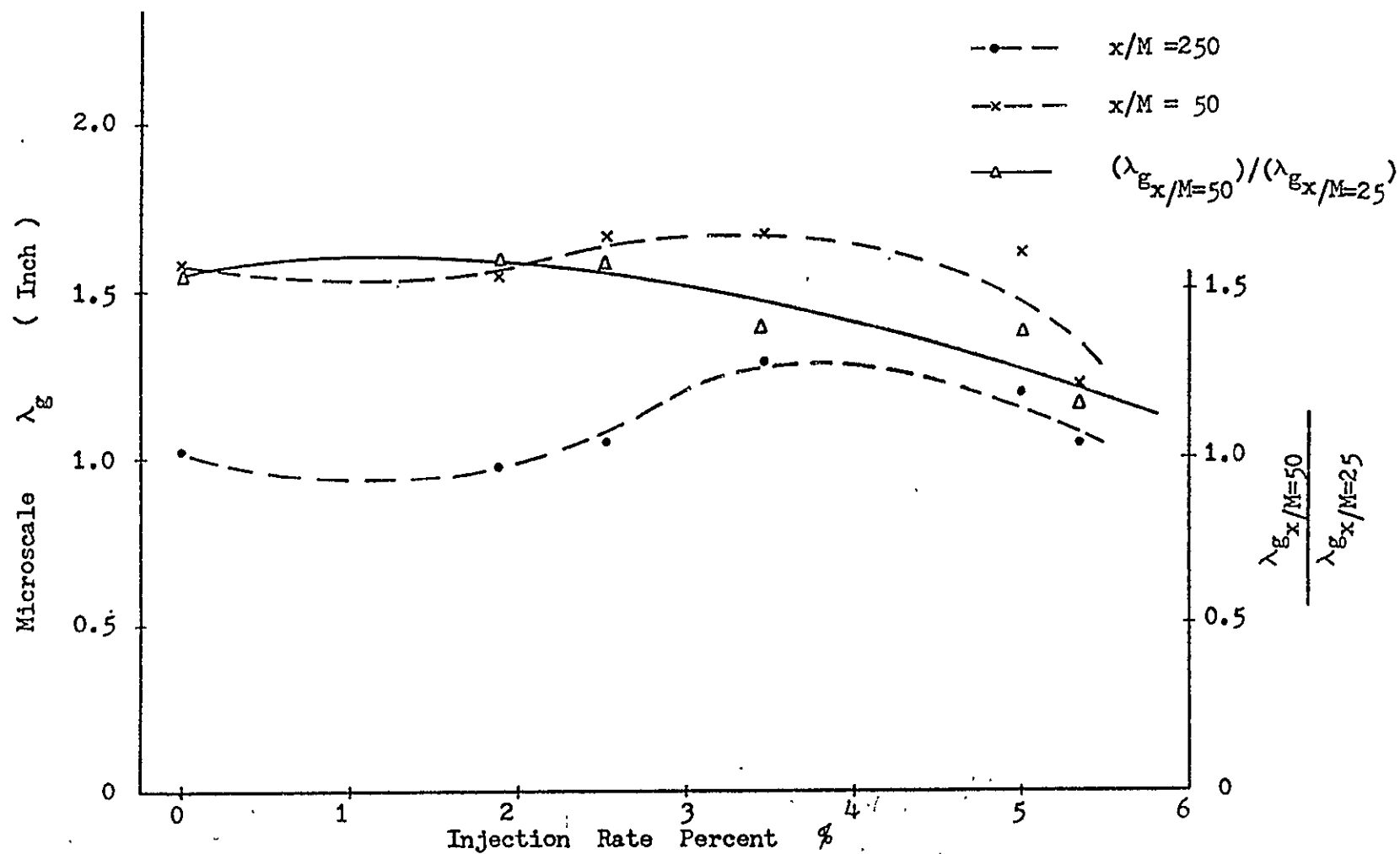
65

Figure 25   MICROSCALES DEDUCED ACCORDING TO $\frac{\overline{u_1^2}}{\overline{U^2}} = a'\left(x/M - x_o/M\right)^{-1} + b'$
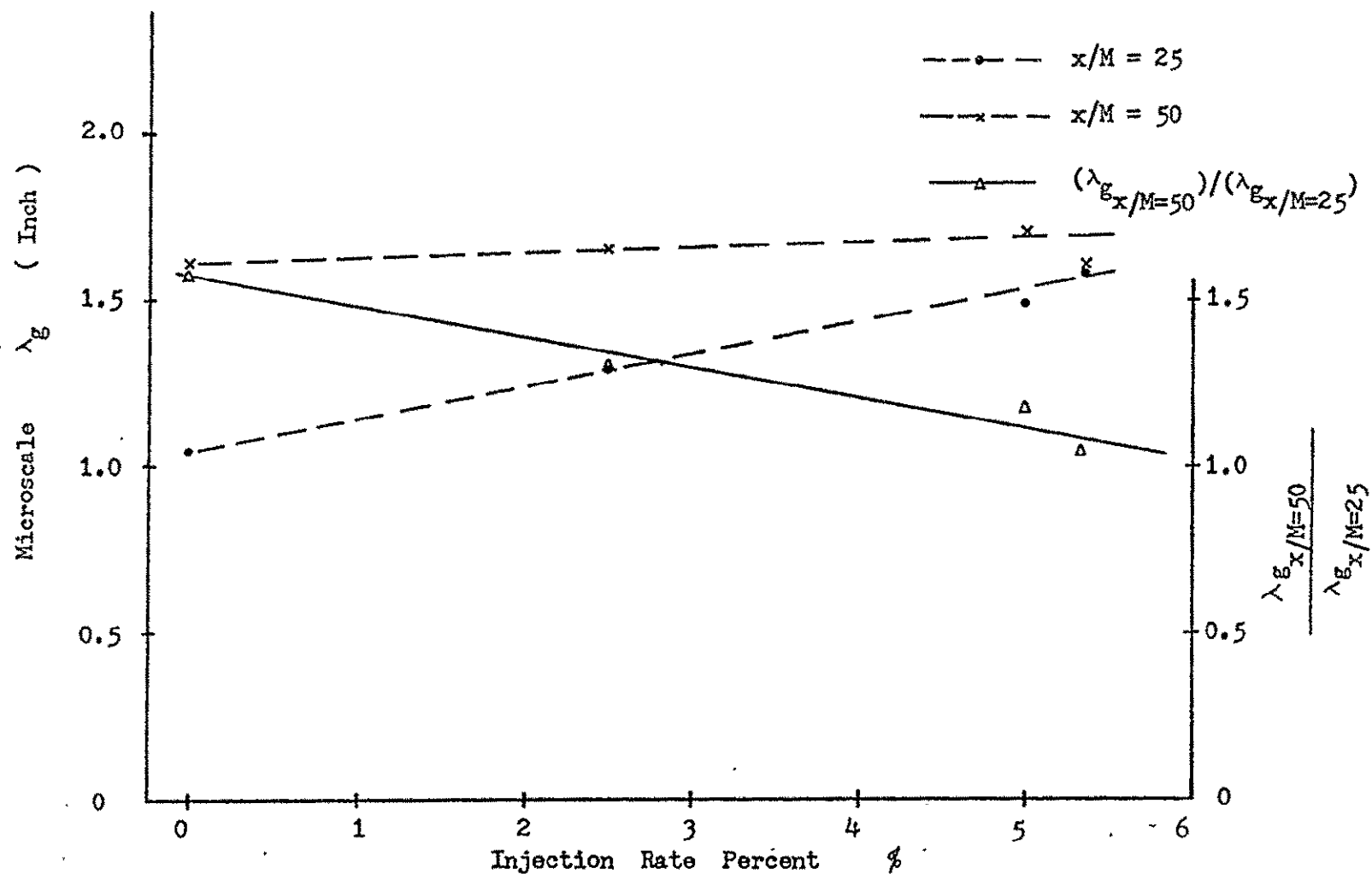
Figure 26   MICROSCALES CALCULATED FROM ENERGY SPECTRA

IRP = 5.34

Peak Velocity

x/M = 31.1   214.92

x/M = 2.15   197.73

x/M = 4.9   219.26

x/M = 10.0   251.67

x = 10 orifice diameter (0.200")

290.89

$\dfrac{r}{R}$

Mean Velocity . $\overline{U}$ (ft/sec)
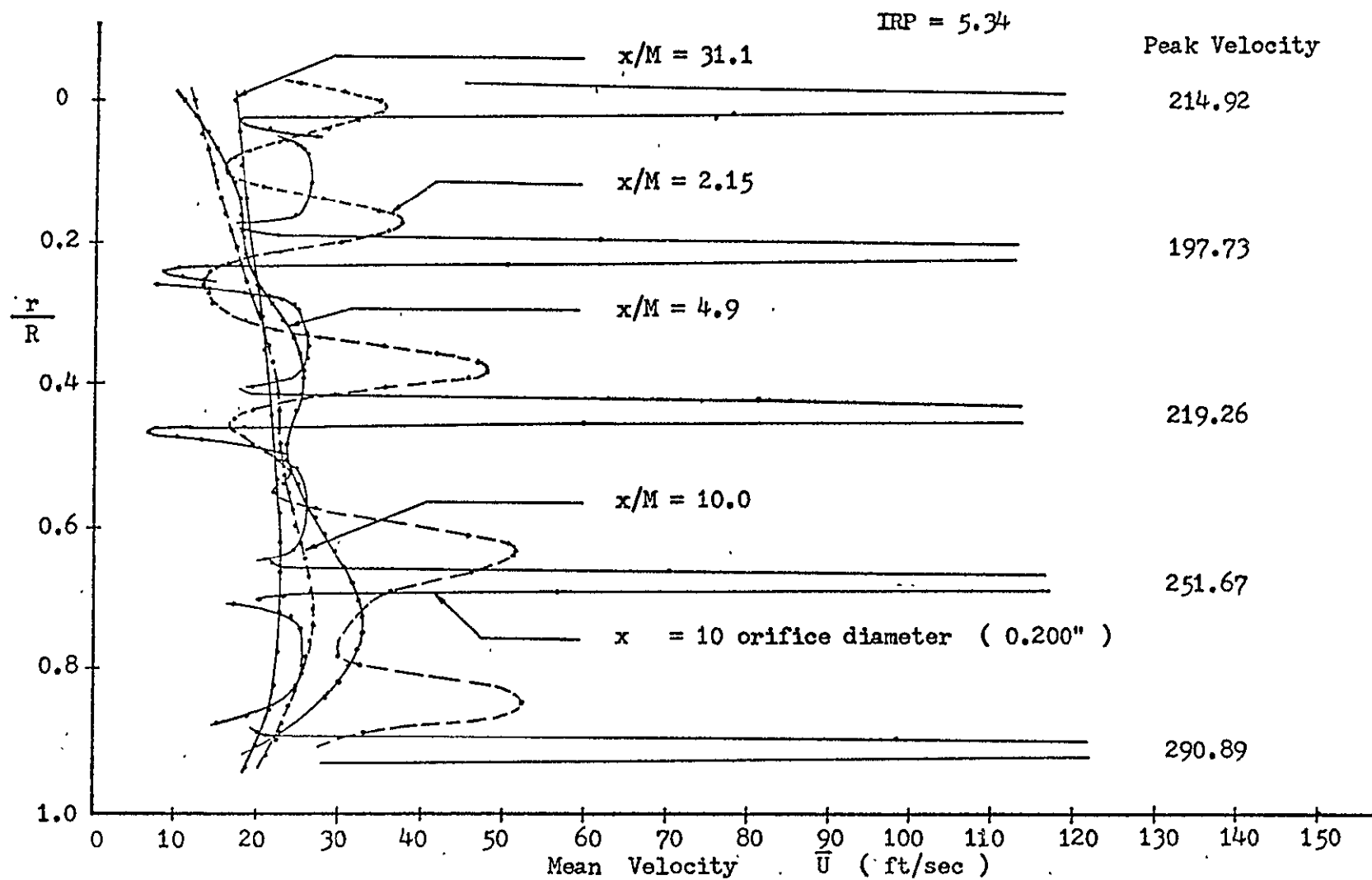
Figure 27   MEAN VELOCITY PROFILE WITH NON-UNIFORM HOLE SIZE ON GRID
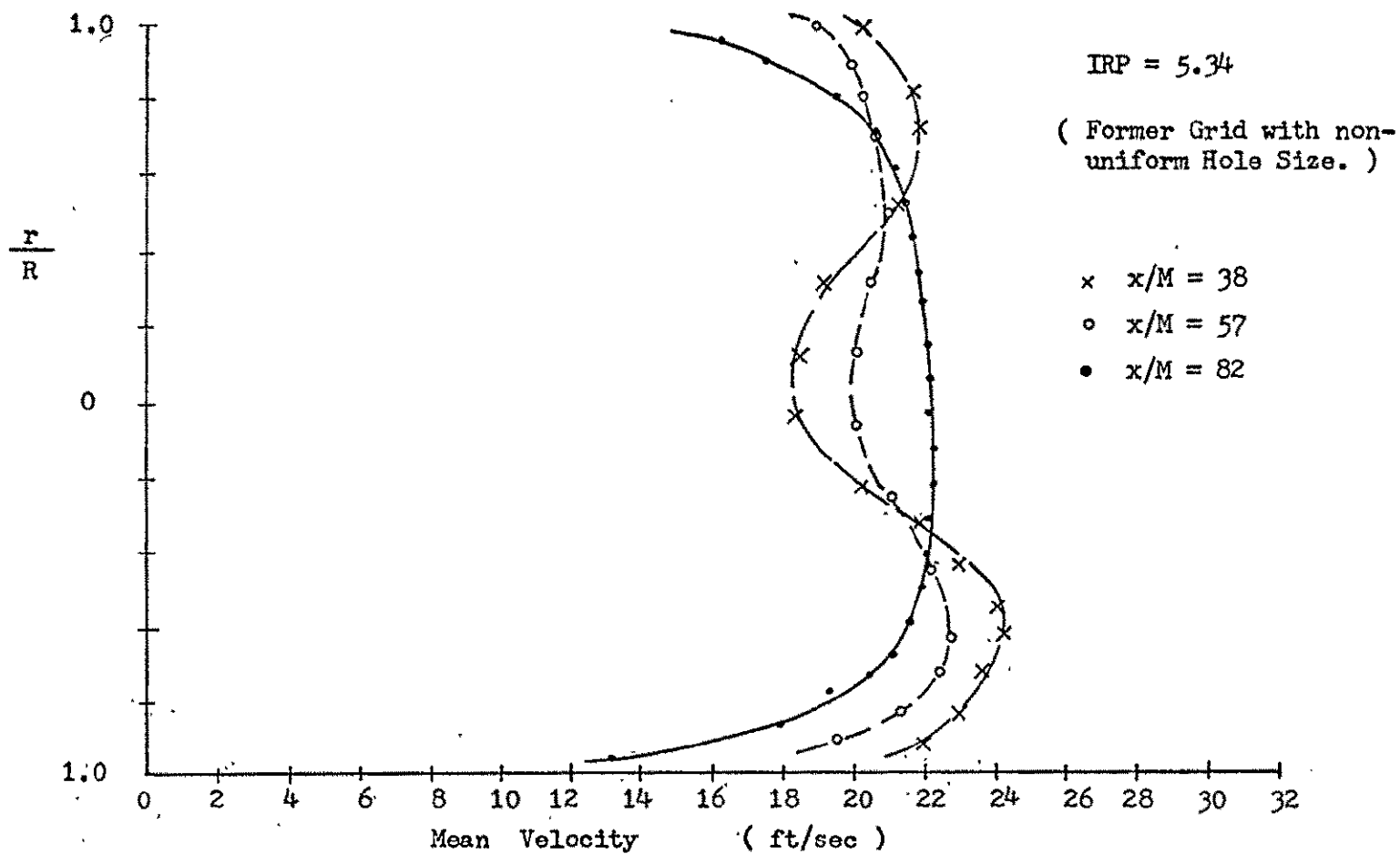
Figure 28   MEAN VELOCITY PROFILE

IRP = 3.44

At 20 Mesh Lengths

(with uniform holes on
  grid: 0.020" D , no extra
  holes near the wall.)

●   Vertical Diameter

o   Horizontal Diameter
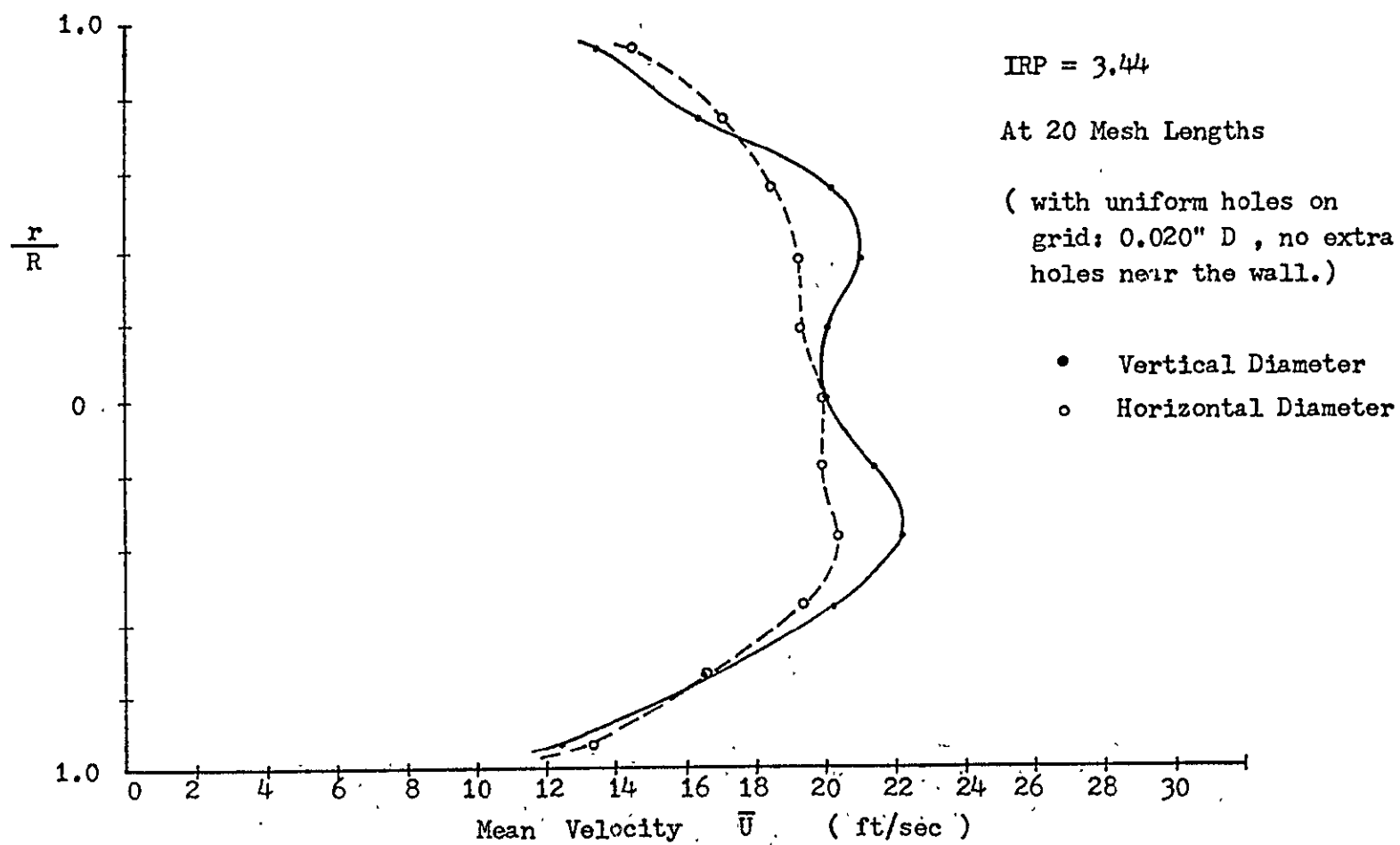
Figure 29 . MEAN VELOCITY PROFILE

IRP = 3.44

At 20 Mesh Lengths

(with uniform holes but 4 center
holes enlarged to 0.022" D., no
extra holes near the wall.)

Traverse Path on Vertical Diameter
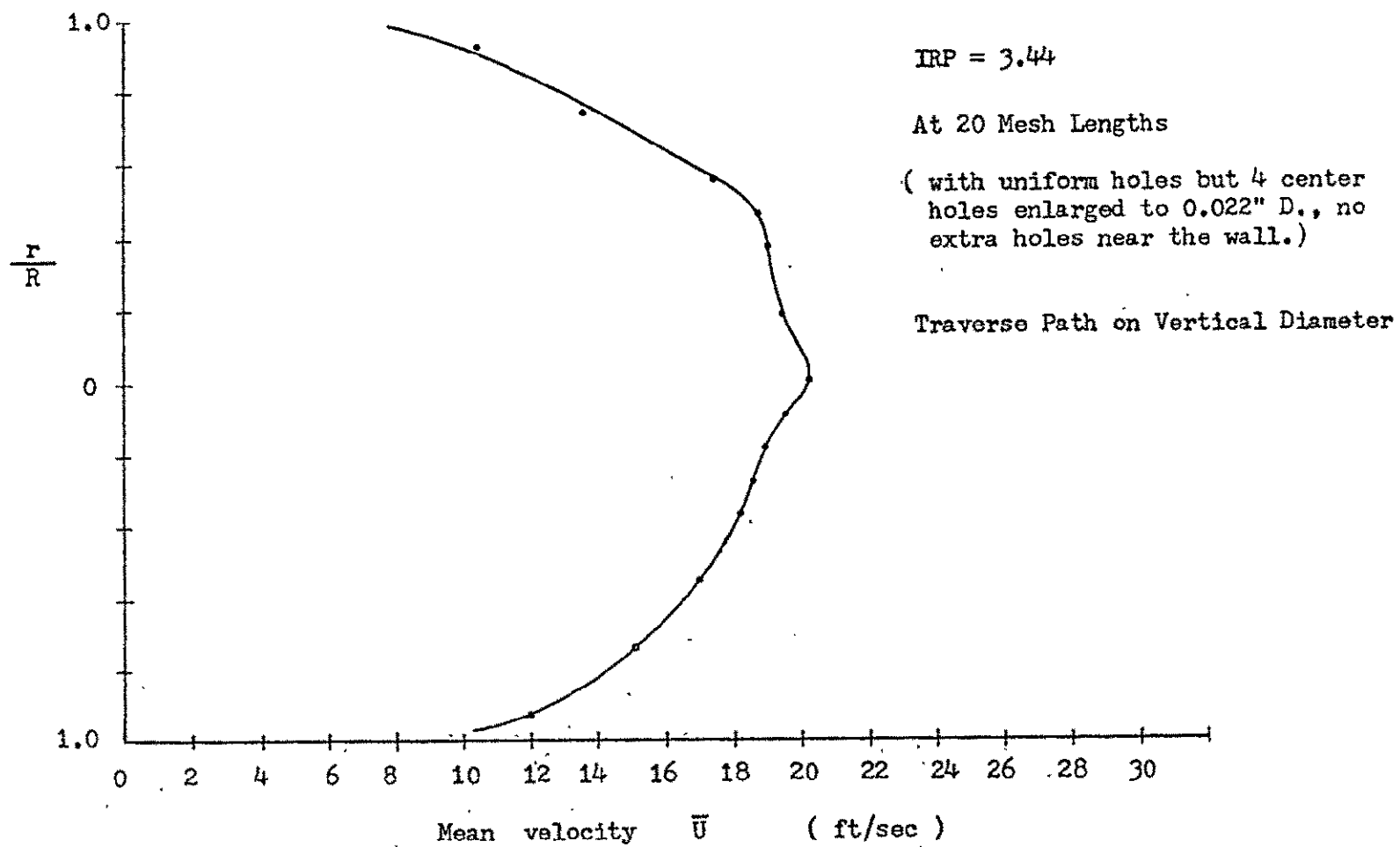
Figure 30   MEAN VELOCITY PROFILE

IRP = 3.44

At 20 Mesh Lengths

(with special grid rods
  providing longer guidence
  in jet direction.)

Traverse Path on Vertical
Diametor.
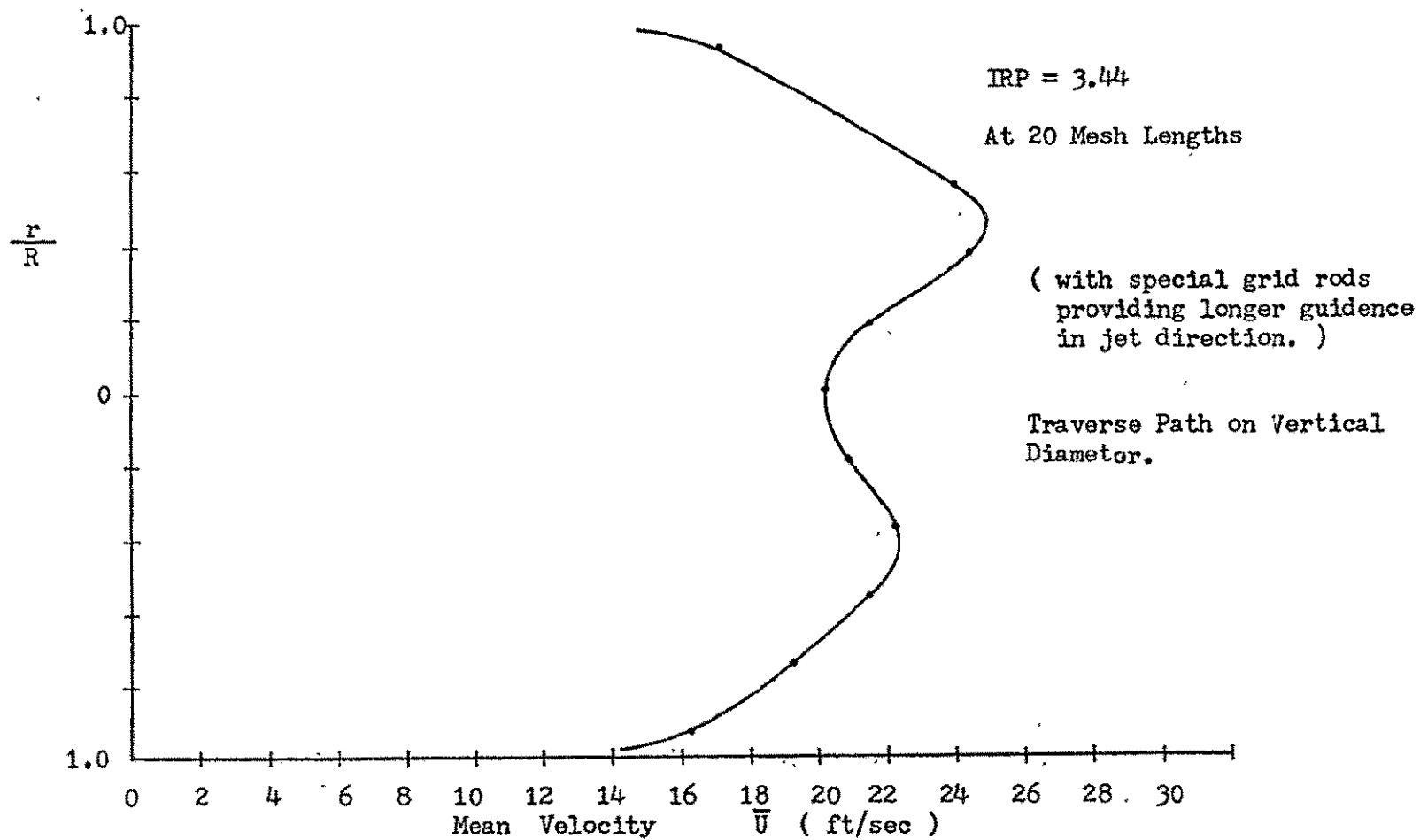
Figure 31 · · MEAN VELOCITY PROFILE

72

IRP= 3.44

At 20 Mesh Lengths

(grid with uniform holes
0.020 in D, and with
extra holes near the
wall.)

●   Vertical Diameter

o   Horizontal Diameter
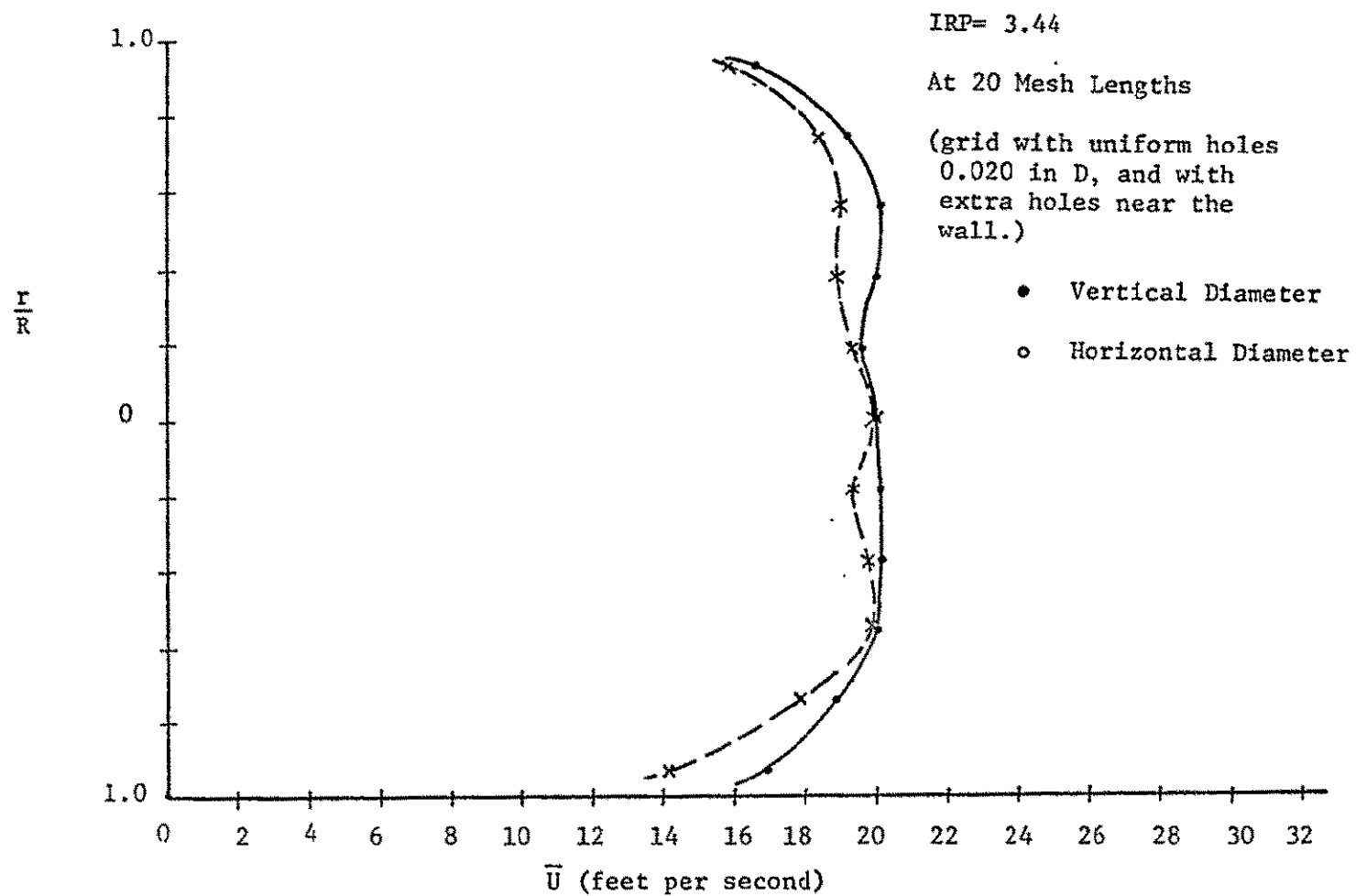
Figure 32   MEAN VELOCITY PROFILE

Figure 33   MEAN VELOCITY PROFILE

IRP = 3.44

At 20 Mesh Lengths

(grid with uniform holes
0.020 in D, without extra
holes near the wall.)

●   Vertical Diameter

○   Horizontal Diameter

$\frac{r}{R}$

$\overline{U}$ (feet per second)

TABLE 1

MICROSCALE AND TURBULENCE REYNOLDS NUMBER DEDUCED ACCORDING TO

$$\frac{\overline{u_1^2}}{\overline{U^2}} = c' \ (\ x/M - x_o/M \ )^{-n}$$

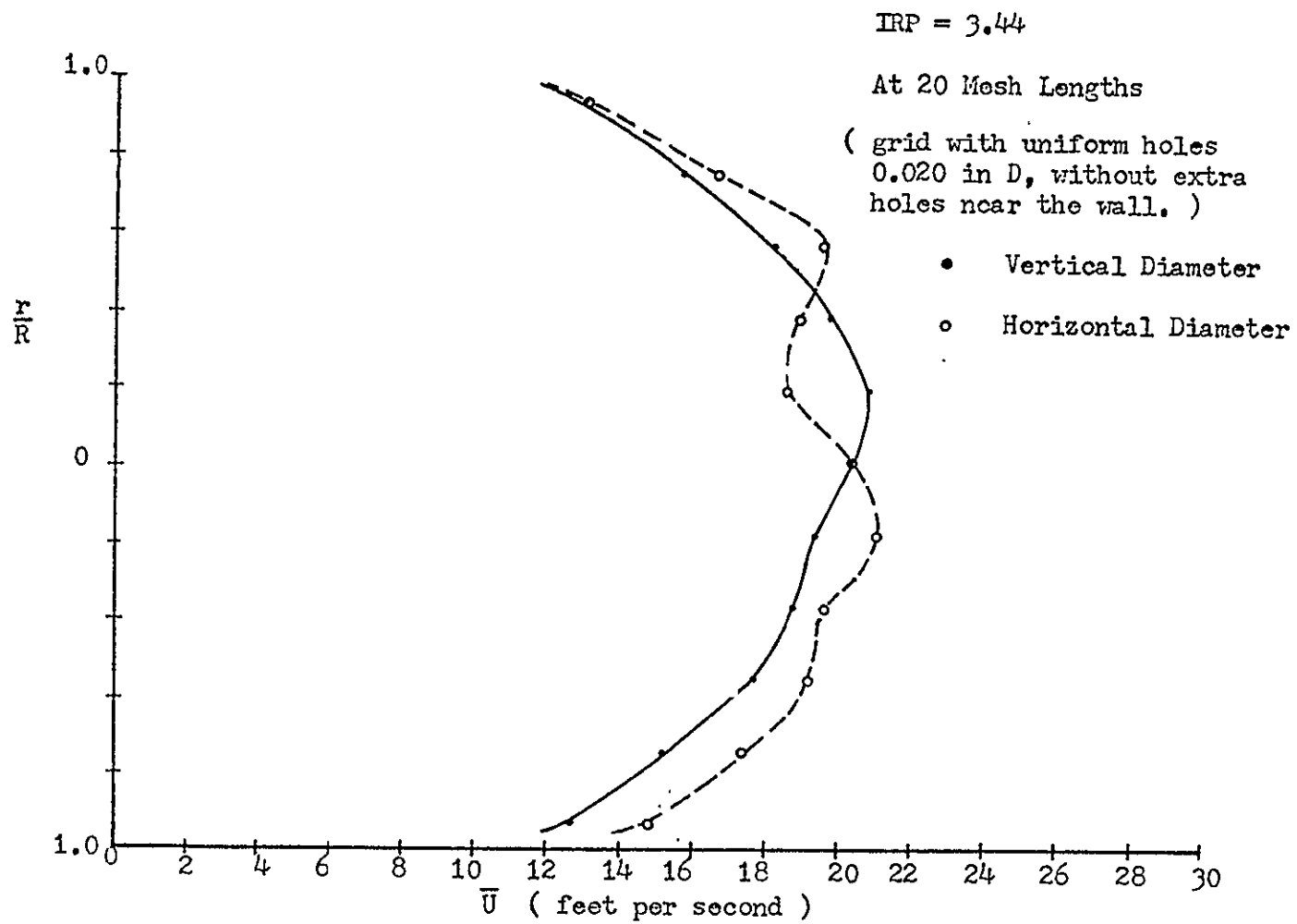| Injection Rate Flowmeter Reading	IRP	$\frac{\overline{U}t_o}{M}$ $\left(\frac{x_o}{M}\right)$	Slope n	g (inch) $\frac{x}{M}=25$	g (inch) $\frac{x}{M}=50$	$\frac{\lambda_{g50}}{\lambda_{g25}}$	$Re_{\lambda g}$ $\frac{x}{M}=25$	$Re_{\lambda g}$ $\frac{x}{M}=50$
0%	0	0	1.45	0.0996	1.141	1.42	19.1	16.3
10%	1.88	5	1.02	0.106	0.159	1.50	25.9	23.7
13%	2.52	8	0.855	0.111	0.168	1.51	32.6	34.7
17%	3.44	−20	2.02	0.113	0.141	1.24	45.9	41.3
20%	4.99	−27.5	2.48	0.110	0.134	1.21	58.4	45.1
23.5%	5.34	−35	3.37	0.1014	0.120	1.18	65.3	41.5

TABLE 2

MICROSCALE AND TURBULENCE REYNOLDS NUMBER DEDUCED ACCORDING TO

$$\frac{\overline{u_1^2}}{\overline{U^2}} = a' \ (\ x/M - x_o/M \ )^{-1} + b'$$

Injection Rate Flowmeter Reading	IRP	$\dfrac{\overline{U}t_o}{M}$ $\left(\dfrac{x_o}{M}\right)$	λ_g (inch) $\dfrac{x}{M} = 25$	$\dfrac{x}{M} = 50$	$\dfrac{\lambda_{g50}}{\lambda_{g25}}$	Re_{λ_g} $\dfrac{x}{M} = 25$	$\dfrac{x}{M} = 50$
0%	0	6.0	0.102	0.158	1.55	19.5	18.3
10%	1.88	7.55	0.0977	0.155	1.59	23.9	23.1
13%	2.52	6.56	0.105	0.166	1.58	31.0	34.3
17%	3.44	−6.18	0.129	0.167	1.39	52.4	48.9
20%	4.99	−0.88	0.117	0.161	1.38	61.8	54.1
23.5%	5.34	−3.86	0.104	0.122	1.17	66.5	41.2

TABLE 3

MICROSCALE AND TURBULENCE REYNOLDS NUMBER DEDUCED FROM ENERGY SPECTRA

| Injection Rate | | λ_g (inch) | | $\dfrac{\lambda_{g50}}{\lambda_{g25}}$ | $Re_{\lambda g}$ | |
Flowmeter Reading	IRP	$\dfrac{x}{M} = 25$	$\dfrac{x}{M} = 50$		$\dfrac{x}{M} = 25$	$\dfrac{x}{M} = 50$
0%	0	0.102	0.158	1.55	19.5	18.3
13%	2.52	0.127	0.162	1.275	37.3	33.4
20%	4.99	0.146	0.167	1.145	77.5	56.2
23.5%	5.34	0.154	0.157	1.02	98.9	53.5